Submitted by:

Walter Frost
Terry S. Paige
Andrew E. Nelius
FWG Associates, Inc.
217 Lakewood Drive
Tullahoma, TN 37388

Submitted to:

NASA Marshall Space Flight Center
Marshall Space Flight Center, AL 35802

FINAL REPORT
Contract NAS8-37893

GUIDE TO MEASUREMENT
OF WINDS WITH
INSTRUMENTED AIRCRAFT

March 25, 1991

Approved:

Dr. Walter Frost, President

TABLE OF CONTENTS

TABLE OF CONTENTS, continued

NOMENCLATURE

$\vec{a}$	Vehicle acceleration
a_x	Acceleration component in the x direction
a_y	Acceleration component in the y direction
a_z	Acceleration component in the z direction
F	An arbitrary function
k	Flow angle sensitivity factor
$\mathbf{L_{BV}}$	Vehicle-centered to body-fixed frame vector transformation matrix
l_x	Displacement component of the gust probe in the x direction
l_y	Displacement component of the gust probe in the y direction
l_z	Displacement component of the gust probe in the z direction
M	Mach number
p	Roll rate
p	Static pressure
p_o	Total pressure
q	Dynamic pressure
r	Yaw rate
R	Ideal gas constant for air
T_o	Total temperature
t	Time
t_o	Initial time
V_a	Airspeed
$\vec{V_a}$	Relative airspeed velocity
$\vec{V_e}$	Vehicle inertial velocity
$\vec{W}$	Wind velocity
α	Angle-of-attack
β	Angle-of-sideslip
κ	Ratio of specific heats
$\Delta()$	Uncertainty of the parameter in ()
τ	Integration dummy variable
ξ_i	A set of independent variables
ϕ	Bank angle
ψ	Heading
θ	Elevation angle
θ	Displacement angle

LIST OF FIGURES

LIST OF TABLES

1.0 INTRODUCTION

Instrumented aircraft have been used for measuring atmospheric winds and turbulence for a number of years. In general, these measurements have been for straight and level flight where limited range instrumentation can be used to measure the parameters of interest and linearized equations can be used to reduce the data. Recently, however, there has been considerable interest in measuring winds along steep flight paths, for example, with respect to STS wind profile measurements in support of day-of-launch activities. The purpose of this report is to review aircraft measurements techniques. Review of past and present applications of instrument aircraft to atmospheric observations is presented. Questions to be answered relative to measuring mean wind profiles as contrasted to turbulence measurements are then addressed. Finally, requirements of instrumentation and accuracy, data acquisition, data reduction, and theoretical and certainty analysis are considered.

Review of Past and Present Applications of Instrumented Aircraft to Atmospheric Observations

The past and present use of instrumented aircraft has been primarily to measure clear air turbulence and winds and turbulence associated with convective storms or gust fronts. The limitations of these aircraft experiments were primarily straight level flight with limited range sensors, limited environmental exposure, simplification of the trigonometric functions of the aircraft attitude and linearized wind equations. A review of the scope and objectives of a variety of aircraft measurement programs as reported in the literature follows.

Telford, Wagner, and Vaziri (1977) point out that the measurement of air motion has now advanced to the stage where routine measurements of the three components of the velocity of the air can be made from aircraft to an accuracy

1

of about 0.3 m/s. They further note that techniques have advanced, from using a simple accelerometer at the center of gravity of the aircraft to give an indication of the updrafts causing the aircraft gust load, to the present inertial platform base systems now is use. Prior to this report, Telford and Wagner (1974) described the measurements of horizontal motion near clouds from aircraft. They described the measurement of air motion for flight in and around small cumulus clouds using a high quality inertial platform and an integrated data handling system. McBean and MacPherson (1976) discuss measurements of the fluctuations of wind, temperature, and humidity using an instrumented aircraft at altitudes from 30 to 300 meters above Lake Ontario. A NAET-33 turbulence research aircraft (a single engine military trainer) was used for the experiment. As instrumented, this aircraft was capable of measuring the three orthogonal components of the true gust velocity and the related fluxes of heat, momentum, and water vapor. Other in flight measurements allowed computation of atmospheric pressure, temperature, humidity, and Doppler wind speed and direction, as well as the altitude, speed, and orientation of the aircraft. A description of the aircraft, its instrumentation, and the data analysis program are available in MacPherson (1973).

Extensive clear air turbulence measurements have been carried out with an instrumented NASA B-57B aircraft. These measurements were part of the NASA Langley Research Center's MAT (Measurement of Atmospheric Turbulence) program. Measurements were carried out to altitudes ranging as high a 15 km. The particular emphasis of this program was to extend power spectral measurements of atmospheric turbulences to wavelengths of at least 9,000 m under several different meteorological conditions. The flight instrumentation system for acquisition of the atmospheric turbulence data is given by Meissner (1976). Some of the measurement results are presented in two volumes. The first volume (Davis, Champine

2

and Ehernberger (1979)) presents the flight planning, operations, and turbulence forecasting aspects. The second volume (Waco (1979)) presents 27 maps of flights of particular meteorological interest with narrative summaries and with synoptic maps and rawinsonde sounding data.

Winebarger (1986) employed a highly instrumented F-106B Delta Dart airplane to make thunderstorm penetrations in the storm hazards program. Details on the F-106B airplane and the criteria used in choosing the airplane for the mission can be found in Fisher, Keyser, Gerald, Deal, Perry, Thomas, and Pitts (1980) and Fisher, Keyser, Gerald, and Deal (1982). The F-106B is equipped with a number of data systems to measure the environmental and electro- magnetic characteristics of thunderstorms during penetration.

The Royal Aircraft establishment, Woodfield and Vaughn (1983), has employed an HS-125 to conduct both windshear and vortex wake studies for many years. In addition to basic instrumentation to measure turbulence in three axis at frequencies up to 20 Hz, the RAE HS-125 was uniquely instrumented with a laser airspeed system (LATAS), which detects windshear several hundred meters ahead of the aircraft and a Marconi AD660 Doppler Velocity Sensor which could be used as the basis of a ground speed/airspeed display.

Rider, Thomson, and Verinder (1971) fitted a Mirage A-376 with a modified nose cone to carry a differential pressure gust probe. The probe was extensively tested in a transonic wind tunnel and the results were confirmed by comprehensive flight test programs. The instrumented Mirage fighter aircraft carried out three flights in an area of severe and low level turbulence. True gust velocities were computed for 540 seconds of recorded data and power spectral energy distributions were determined which confirm various levels of turbulence.

Crooks, Hoblit, and Prophet (1967) describe high altitude clear air turbulence

3

(HICAT) flight investigations. A digital instrumentation system for the measurement of CAT in the wavelength range from about 100 ft to 60,000 ft was utilized. The program effort required the measurement of CAT velocity components at altitudes of 45,000 to 75,000 ft in seven geographical areas. Instrumentation carried aboard the HICAT aircraft, and Air Force U2 consisted of a PCM system, a inertial navigation system, aerodynamic and aircraft response sensors (including a fixed vane gust probe), an oscillograph record, and a digital magnetic tape recorder. The program objective was to determine the statistical characteristics of high altitude CAT so as to improve structural design criteria. Time histories and power spectra are provided in Volume I of the report while meteorological data and flight track maps are included in Volume II.

Frost, Chang, and Ringnes (1987) present the analysis of turbulence measured across the airfoil of a Cambera B-57 aircraft. The aircraft was instrumented with probes for measuring winds at both wing tips and at the nose. Statistical properties of the turbulence are reported. These consist of the standard deviations of turbulence measured by each individual probe, standard deviations and probability distributions of difference in turbulence measured between probes, and auto and two-point spatial correlations in spectra.

Ganzer, Joppa, and van der Wees (1977) used a similarly equipped aircraft to measure turbulence. A Beechcraft D-18S, a low wing all-metal semi-mono-coque, aircraft was used. The aircraft was instrumented to measure and record the variables necessary for the calculation of the turbulence velocity in longitudinal, lateral, and vertical directions at the wing tips of the aircraft. A detailed description of the instrumentation and calibration is presented in the report.

Kraus, Hacker, and Hartmann (1990) carried out research flights in the Coorong coastal area of South Australia to investigate sea breeze fronts. The flights yielded

data sets of the structure of the fronts in the cross frontal direction with a spatial resolution of approximately three meters. The study is focused on the budgets of sensible and latent heat in the vicinity of the front and on frontogenesis/frontolysis processes which are closely related to budget considerations. A light, well instrumented aircraft developed by the Finders Institute for Atmospheric and Marine Sciences (FIAMS) was used. The aircraft, a GROB G109B, along with its instrumentation and capabilities are described in detail by Hacker and Schwerdtfeger (1988). Air temperature was measured using a fast PT100 sensor, humidity was measured with an A.I.R., Inc. Lyman-α hydrometer and a Meteolab dewpoint mirror. The three dimensional wind vector was sensed by a system consisting of a five-hole probe, a Rockwell-Collins AHS-85 altitude and heading reference system and a Trimble TANS GPS navigation system (satellite based Global Positioning Systems). The horizontal wind vector was determined from an algorithm which utilized high resolution integrated inertial data from the AHRS with the stable low resolution data from the GPS navigation system. The accuracies of the instrumentation were reported as approximately 0.02 K^o for temperature and 0.02 g/kg for humidity. For the wind vector, the reported accuracies were 0.9 m/s for the horizontal wind and a few centimeters per second for the vertical wind.

Lenschow, Li, Zhu, and Stankov (1987) present measurements of the stable stratified nocturnal boundaries layer obtained with the Queen Air NCAR aircraft during the severe environmental storms in a mesoscale experiment (SESAME). The cases presented were obtained over rolling terrain in central Oklahoma, with a mean slope of about 0.003. The results are reported to be in general agreement with previous modeling and observational studies for the mean and turbulence structure of the nocturnal boundary layer. An exception was that the eddy diffusivity of heat and consequently the flux Richardson numbers are less than expected.

5

Stromberg, Mill, Choularton, and Gallagher (1989) made airborne measurements of stably stratified airflow over the Pennines using an instrumented glider. The parameters measured in flight were air temperature, airspeed, vertical acceleration, and vertical velocity. Airspeed and pressure altitude were measured using sensitive pressure transducers and resolution was reported as better than one millibar for altitude and approximately one meter per second for airspeed. Vertical velocity of the air was measured using the sail plane variometer system. In this system, the inherent sink rate at a particular speed was automatically subtracted from the total signal to give the vertical velocity of the air itself. The resolution was better than 1 meter per second and accuracy to within plus or minus 0.1 meter per second.

Lenschow and Johnson (1968) made concurrent airplane and balloon measurements of atmospheric boundary layers structure over a forrest. Mean wind profiles up to a height of 2,000 m and supporting surface layer measurements were observed. The airplane measurements of vertical and horizontal velocity were obtained from a pressure differential gust probe mounted on a boom on the nose of a twin engine Cessina 310 airplane. Further description of the airplane is provided in Dutton and Lenschow (1962) and Lenschow (1965). The system removes airplane motions from the air vertical velocity measurements by measuring the pitch angle and vertical acceleration of the airplane. The technique is limited to wavelengths of less than 1.3 km for airspeeds of 70 m/s primarily because of drift in the gyro used to measure pitch angle. The velocity fluctuations were filtered with an RC high-pass filter with a time constant of 3.0 seconds which results in a half power wavelength of 1.3 km. Temperature was measured with a thermal couple mounted on the boom less than 50 cm behind the gust probe sensors. The time constant of the thermal couple is about 1 second.

6

Benjamin (1989) reports an objective analysis scheme for meteorological variables on constant potential temperature surfaces. The analysis uses the form of multivarient statistical interpretation and is designed to retain mesoscale detail in various observations including rawinsonde, surface, aircraft, satellite, and wind profiler data while combining them with a forecast background field. Commercial aircraft observations of temperature and wind were used. Aircraft reports of icing were converted into approximate observations of 100% relative humidity.

Parish and Bromwich (1989) report instrumented aircraft observations of the katabatic wind region near Terra Nova Bay. Two aircraft missions were flown to sample the boundary layer dynamics associated with the intense katabatic winds. An LC-130 instrumented aircraft developed for meteorological research was utilized. The data system is described in Renard and Foster (1978) and an itemization of the onboard instrumentation is given in Gosink (1982). The LC-130 is equipped to record a total of 18 data channels of meteorological and navigational parameters at 1 second intervals on high density magnetic tapes.

Gage and Nastrom (1986) present a theoretical interpretation of the wave number spectra of winds and temperature obtained from an analysis of data from over 6,900 flights during the global atmospheric sampling program (GASP). Data were collected automatically on specially instrumented Boeing 747 aircraft in routine commercial service, with most measurements made in the altitude range between 9 and 14 km. For most flights the flight interval is 75 km and the length scale sampled range to about 5,000 km. The 6,900 flights in the GASP data base were made during all seasons and covered a wide variety of latitudes and longitudes.

The proceeding summarizes types of aircraft measurement programs which have been carried out using a range of aircraft from highly instrumented aircraft, to gliders to commercial aircraft of "opportunity". The principle of extracting

7

winds from the measurements, however, is basically the same. This principle is described in the next section. Essentially, it is a matter of measuring the aircraft inertial velocity vector and the velocity vector of the air relative to the aircraft. The difference is the wind velocity vector. The parameters which need to be measured and a variety of the instrument types used are described in the next section.

2.0 INSTRUMENTATION AND PRINCIPLES OF WIND MEASUREMENT

The principle and governing equations relative to the measurement of winds from an aircraft are well documented (for example see Axford (1968); Lenschow (1986); Frost, Chang, and Ringnes (1987)). The basic physical principle is embodied in the vector relationship

$$\vec{W} = \vec{V_e} - \vec{V_a} \tag{2.1}$$

where $\vec{W}$ is the wind vector, $\vec{V_e}$ is the aircraft inertial velocity vector and $\vec{V_a}$, is the relative airspeed vector. The aircraft therefore must be equipped with instruments that measure ground speed (i.e., inertial) and the speed of the air relative to the aircraft. Expressing the vectors $\vec{V_e}$ and $\vec{V_a}$ in an appropriate coordinate system to provide windspeeds in the earth's coordinate system requires that the 6 degree-of-freedom motion of the aircraft be measured. The system of equations required to reduce the aircraft measurements into components of windspeed are thus complex. They have been fully derived, however, and are reported in the previously mentioned references (Frost, Chang and Ringnes (1987) is an example). This derivation is partially reproduced in Appendix A.

The fully expanded form of the system of equations for computing the wind velocity vector components in the earth's frame of reference is:

$$
\begin{aligned}
W_N = - \overline{V}[&\cos\alpha\cos\beta\cos\Psi\cos\theta + \sin\beta(-\sin\Psi\cos\phi + \cos\Psi\sin\theta\sin\phi) \\
&+ \sin\alpha\cos\beta(\cos\Psi\sin\theta\cos\phi + \sin\Psi\sin\phi)] + V_N \\
&- l_x(\dot{\Psi}\sin\Psi\cos\theta - \dot{\theta}\cos\Psi\sin\theta) \\
&+ l_y[\dot{\theta}\sin\phi\cos\theta\cos\Psi + \dot{\phi}(\sin\phi\sin\Psi + \cos\phi\sin\theta\cos\Psi) \\
&- \dot{\Psi}(\cos\phi\cos\Psi + \sin\theta\sin\phi\sin\Psi)] \\
&+ l_z[\dot{\theta}\cos\phi\cos\theta\cos\Psi + \dot{\phi}(\cos\phi\sin\Psi - \sin\phi\sin\theta\cos\Psi) \\
&+ \dot{\Psi}(\sin\phi\cos\Psi - \sin\theta\cos\theta\sin\Psi)]
\end{aligned} \tag{2.2}
$$

9

$$W_E = -\overline{V}[\cos\alpha\cos\beta\sin\Psi\cos\theta + \sin\beta(\cos\Psi\cos\phi + \sin\Psi\sin\theta\sin\phi)$$
$$+ \sin\alpha\cos\beta(\sin\Psi\sin\theta\cos\phi - \cos\Psi\sin\phi)] + V_E$$
$$- l_x(\dot{\theta}\sin\theta\sin\Psi - \dot{\Psi}\cos\phi\cos\theta)$$
$$+ l_y[\dot{\theta}\sin\phi\cos\theta\sin\Psi + \dot{\phi}(-\sin\phi\cos\Psi + \cos\phi\sin\theta\sin\Psi) \qquad (2.3)$$
$$- \dot{\Psi}(\cos\phi\sin\Psi - \sin\theta\sin\phi\cos\Psi)]$$
$$+ l_z[\dot{\theta}\cos\phi\cos\theta\sin\Psi - \dot{\phi}(\cos\phi\cos\Psi + \sin\phi\sin\theta\sin\Psi)$$
$$+ \dot{\Psi}(\sin\phi\sin\Psi + \sin\theta\cos\phi\cos\Psi)]$$

$$W_Z = -\overline{V}[-\cos\alpha\cos\beta\sin\theta + \sin\beta\cos\theta\sin\phi + \sin\alpha\cos\beta\cos\theta\cos\phi]$$
$$+ V_Z + l_x\dot{\theta}\cos\theta - l_y[\dot{\theta}\sin\phi\sin\theta - \dot{\phi}\cos\phi\cos\theta) \qquad (2.4)$$
$$- l_z[\dot{\theta}\cos\phi\sin\theta + \dot{\phi}\sin\phi\cos\theta]$$

where W_N, W_E, and W_Z represent the north, east, and vertical components, respectively, of the wind velocity vector. Inspection of these equations shows the variables required in computing wind velocity vector components are those listed and defined in Table 2.1.

Sections 2.1 and 2.2 describe the basic principles of the various sensors available for making the required measurements and the advantages and disadvantages of different types. However, a review of overall systems for measuring wind as applied to different aircraft as reported in the literature is given first. Brown, et al. (1974) describes a research gust probe system. The system was installed on a DC-6 aircraft. It was initially developed and used in the Barbados oceanographic and meteorological experiment (BOMEX). A digital instead of an analog recording system was subsequently added and the system was used in the International Field Year on the Great Lakes project (IFYGL). The system was essentially composed of a fixed vane sensor mounted on a noseboom. The fixed vane sensor is reported in Crooks, et al. (1976) and consists of a vertical sensor (α-vane) and a lateral sensor (β-vane) attached to a specially constructed strain gauge beam. Ambient pressure is sensed by a Conrac type 555 T-1 absolute pressure transducer/servo assembly. A thermistor temperature probe assembly and a microwave cavity instrument to

10

Table 2.1   **Variables required for wind computations.**

Symbol	Description
t	time(sec)
α	angle of attack (rad)
β	sideslip angle (rad)
ϕ	roll angle (rad)
θ	pitch angle (rad)
Ψ	heading angle (rad)
$\dot{\phi}$	roll rate (rad/sec)
$\dot{\theta}$	pitch rate (rad/sec)
$\dot{\Psi}$	yaw rate (rad/sec)
P	static pressure (Kp_a)
T	temperature (Kelvin)
LAT	latitude (deg)
LONG	longitude (deg)
V_N	north-south airplane inertial velocity (m/sec)
V_E	east- west airplane inertial velocity (m/sec)
V_Z	vertical airplane inertial velocity (m/sec)
$\overline{V}$	true airspeed (m/sec)

measure index of refractivity are also mounted on the noseboom. Two Statham strain gauge accelometers were mounted on the boom to sense normal and lateral boom accelerations. A third Statham strain gauge accelometer which was temperature controlled was used to sense longitudinal accelerations of the aircraft. A Litton LTN-51 inertial navigation system provided the basic information regarding aircraft motion with respect to the earth. Signals recorded from the INS were vertical acceleration, roll, and pitch. Aircraft angular motions rates of pitch, roll, and yaw were provided by gyros. Elevator position was also monitored. A model MC013 data acquisition system provided means of measuring up to 64 analog voltages at sample rates up to 3,200 samples per second (50 scans per second of 64 inputs); thus provided a recording of all digital forms along with the time, day of the year and manually entered header data. Recording was carried out on a 7-track gapped tape, IBM compatible.

Gamo, et al. (1975, 1976), Yamamoto, et al. (1977), and Yokoyama, et al. (1977a, 1977b) describe an airborne measurement system mounted on a Cessna 207 aircraft. The system consisted of a hotwire anemometer used for measuring longitudinal velocity fluctuations (observations are made with the aircraft flying parallel to the wind), sonic anemometer used to measure vertical fluctuations, horizontal vanes used to measure the lateral component of the wind, thermistor psychrometer used to measure mean temperature and humidity, sonic thermometer used to measure temperature fluctuations, thermocouple thermometer also used to measure temperature fluctuations, and a radiation thermometer used to measure surface temperature. The airplane's pitching, rolling, and yaw angles and vertical, lateral, and longitudinal accelerations were measured with an inertial platform system.

Scott, et al. (1989) describes the meteorological measurement system incorporated on the NASA ER-2 aircraft. The meteorological measurement system (MMS)

consists of a special inertial navigation system, a differential pressure system installed in the nose of the aircraft, a data acquisition system, and airdata instrumentation. The high resolution INS is especially configured with a data bus which is updated at 25 Hz. The differential pressure system provides sensitive measurements of the airflow angles (angle-of-attack and angle-of-sideslip). The data acquisition system meets the requirements to sample, control, and process 45 parameters at a sampling rate up to 40 Hz. per parameter and store the data in a tape recorder (20 MB.) and a hermetically sealed Winchester hard disk (10 MB.). Special and redundant instrumentation for aircraft and pressure measurements are also installed on the aircraft.

Poellet (1990) describes the University of North Dakota, Cessna Citation II, airborne weather research system. Parameters of temperature, dewpoint and pressure are measured by relatively standard methods using state-of-the-art instrumentation. The position measurements are based on a Litton LTN-76 inertial navigation system. Air motion measurements are derived from measurements of acceleration pitch, roll and yaw combined with angles-of-attack and sideslip and indicated airspeed. The instrumentation pallet also includes radiation instrumentation, cloud microphysics measurement equipment, and a forward or side looking video camera to provide a visual record of flight conditions. Data are sampled at various rates from 1-24 times per second. The sampling is controlled by the onboard computer system which also displays the data in real time.

A number of other reports discuss evaluation of different instrumentation for use in atmospheric measurement programs. Murrow and Rhyne (1975) describe flight instrumentation for atmospheric measurements; Lenschow and Kelley (1975) discuss atmospheric mesoscale measurements from aircraft including instrumentation and measurement techniques; Bjarke and Ehernberger (1989) discuss inflight

13

techniques for wind measurements in support of the space shuttle program, and Lenschow (1986) discusses aircraft measurements in the boundary layer.

The following section describes the physical principles of some of these instruments used in the aforementioned systems.

2.1 Relative Airspeed

The relative airspeed vector requires a magnitude and direction measurement. Magnitude is generally calculated with pitot measurements and direction with either flow vanes or differential pressure transducers.

Relative airspeed magnitude is computed from the equation

$$V_a = \left(\frac{p_o}{p}\right)^{-\frac{k-1}{2k}} \sqrt{kRT_o} \sqrt{\left[\left(\frac{p_o}{p}\right)^{\frac{k-1}{k}} - 1\right]\left[\frac{2}{k-1}\right]} \qquad (2.5)$$

where the measured parameters are total pressure, p_o, static pressure, p, and total temperature, T_o. Figure 2.1 illustrates schematically the measurements required to determine airspeed magnitude, and a detailed derivation of Equation 2.5 is given in Appendix A.

The direction of the air relative to a probe is fixed by the angle-of-attack, α, and sideslip angle, β. These angles are generally determined with either a differential pressures flow angle probe or vanes. A comparison of the flow angle differential pressure probe versus vane measurements is given in Appendix A. The pressure differential flow angle probe is illustrated in Figure 2.2(a) and the vane system in Figure 2.2(b).

A variety of types of flow angle measurement techniques are reported in the literature. Gracey (1958) reviews and summarizes methods of measuring angle-of-attack on aircraft. Three types of angle-of-attack sensing devices – the pivoted vane, the differential pressure tube, and the null seeking pressure tube – are presented. Flight data on the position errors for three sensors locations (ahead of the

14
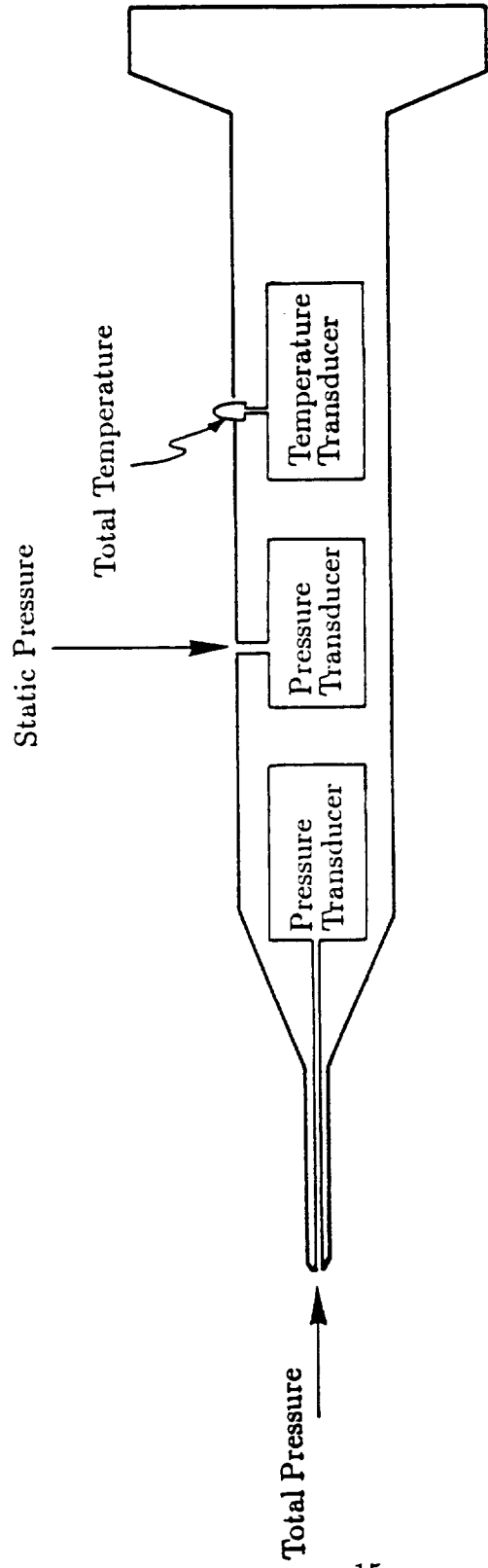
Figure 2.1 Physical quantities required for airspeed measurement.

- - - - ►   Projected body-fixed airflow vector

α Angle-of-attack

β Sideslip angle

Pressure ports

α

β

Flow angle probe

Orthogonal
reference planes
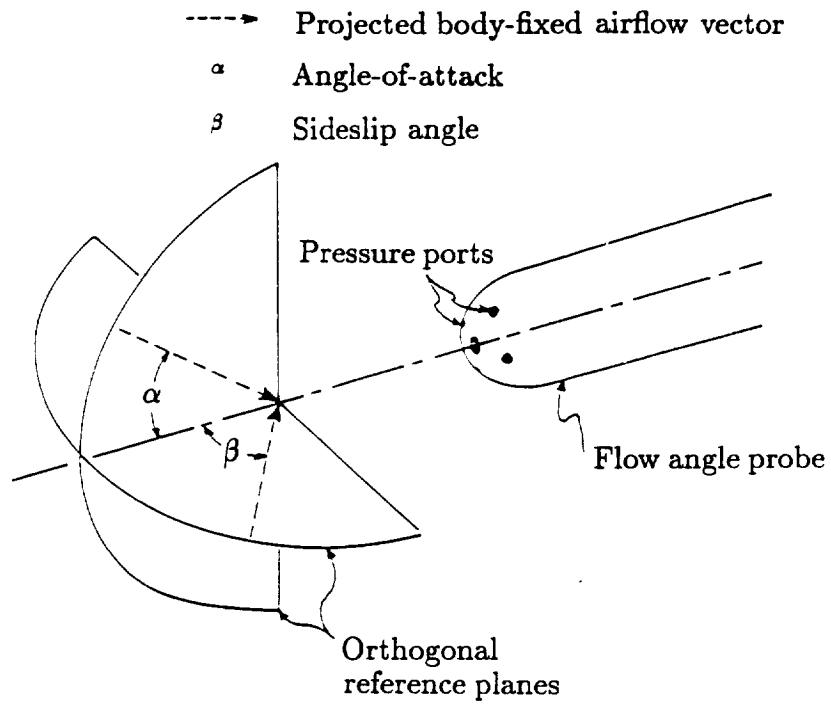
a) Differential pressure probe
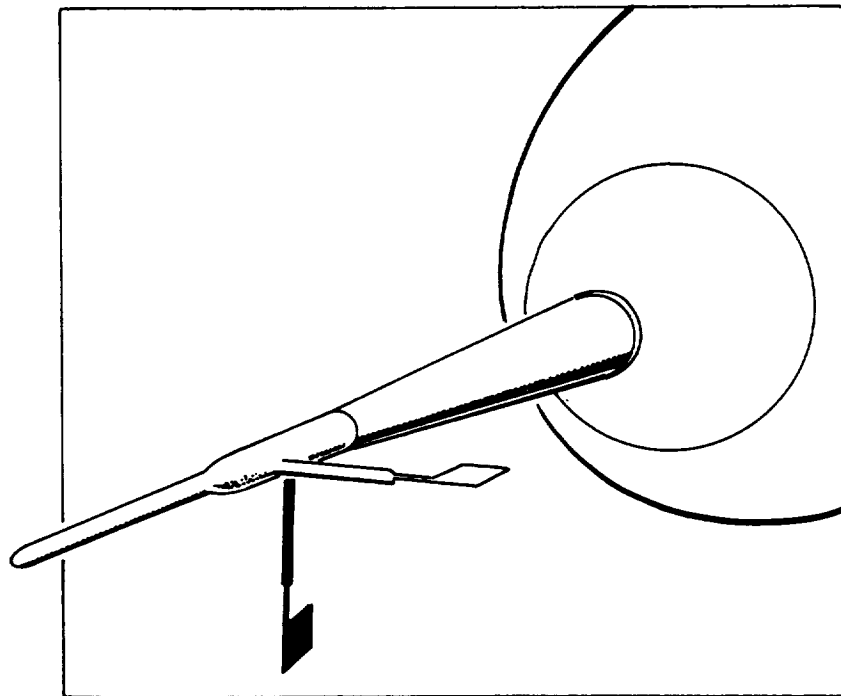
b) Vanes

Figure 2.2   **Angle-of-attack and sideslip angle type sensors.**

16

fuselage-nose, ahead of the wing- tip, and on the forebody of the fuselage) are also presented. Gracey reports that for operations throughout the subsonic, transonic, and supersonic speed ranges, a position ahead of the fuselage-nose will provide the best installation. Moreover, if the shape of the fuselage-nose is not too blunt, the position error will be essentially zero when the sensor is located 1.5 or more fuselage diameters ahead of the fuselage. The report concludes with various methods of calibrating angle-of-attack installations in flight.

Lenschow (1971) describes two types of vanes that were used to measure the angle of airstream with respect to an aircraft. One type is a rotating vane that is free to align itself with the airstream and the angle is sensed by the angle transducer. The other type is constrained from rotating and the angle is obtained by measuring the force exerted on the vane by the airstream and dividing by the pitot-static pressure. It is reported that the free vane measures the angle directly and is not sensitive to acceleration while the constained vane has a faster response time and has no bearing friction. With an aircraft speed of 70 m/s, both vanes are able to resolve changes in angles of less than 0.02 degrees, which corresponds to a gust velocity of about 2 cm/s, and to respond to within 5% of a step function change in angle in a distance of less than 5 meters.

Barna and Crossman (1976) carried out experimental studies of the aerodynamic performance and dynamic response of flow direction sensing vanes. Systematic investigations of a variety of aerodynamic surfaces were carried out. Single vanes consisting of flat plates of various plan forms having aspect ratios between 0.5 and 5; bi-vanes with aspect ratio of 2.5; various cones and box vanes; and various cruciform configurations were all studied. Lift and drag force measurements and damping and frequency tests were all performed under a variety of flow conditions in a wind tunnel.

17

Lenschow, et al. (1978a) reports the status of air motion measurements on a NCAR aircraft for three types of gusts probe sensors. Measurement of airflow angles were studied for: a fixed "constained" vane which measures the force of the airstream on the vane surface at varying flow angles, a rotating vane which aligns itself with the airstream, and a differental pressure probe which senses the pressure difference across a symmetric set of ports at various flow angles. They conclude that although the frequency response of most of the gust probe sensors is sufficient for turbulence flux measurements, it is not sufficient for measuring high frequency characteristics of turbulence such as direct measurements of viscous dissipation or the variation in turbulence intensity on very small scales. Lenschow, et al. (1978b) therefore studied a hot-wire anemometer system capable of measuring two frequencies of several kilohertz. The sensing elements of the hot-wire anemometer were typically fine tungsten wires 4 μm in diameter and 1.25 mm long. These were mounted transverse to the airflow on a probe attached to the aircraft nose- boom. The nose-boom mount permitted velocity measurements within a few tens of centimeters of the standard gust probe sensors at a location that is relatively free of upwash effects induced by flow around the aircraft. Lenschow, et al. concluded that the hot-wire anemometer system is an effective means of extending aircraft velocity measurements to high frequencies and small space scales and that the commercial tungsten wire probes were found to be sufficiently strong so that breakage was not a severe problem in clear air. Further applications of the hot-wire system were reported to consist of measurements of the vertical and transverse velocity components with multiple wires placed at angles to the flow. Jacobsen (1977) reports use of a three-wire array mounted on a trailing aircraft to measure vorticities generated by a large aircraft.

The NASA ER-2 aircraft uses the nose of the aircraft as a differential pressure

transducer system. This concept has been studied by others. Hillje and Tymms (1980) investigated the use of a biconic spike probe on the nose of the space shuttle external tanks to evaluate ascent airdata. Pressure measurements were calibrated to obtain vehicle speed, attitude (relative to the local air mass) and dynamic pressure during launch. They describe the geometry of the ascent airdata system and results of wind tunnel tests carried out for calibration. They concluded that from wind tunnel calibrations, a 30 degree/10 degree spike measured pressure could be converted to the desired airdata parameters for post flight analysis. A typical value for the angle-of-attack error for a Mach range between 0.6 and 1.0 and an $\alpha = 3$ degrees was estimated at $\pm$ 0.32. Other accuracies of the system are presented in the paper. Hillje and Nelson (1981) provide additional data on the space shuttle ascent airdata system.

Brown, Friehe, and Lenschow (1983) describe the use of pressure fluctuations on the nose of an aircraft for measuring the air motion. Measurements of angle-of-attack and sideslip angles and dynamic pressure are described. The sensing probe consisted of an array of five pressure holes in the standard radome of a twin jet research aircraft. Comparisons with air motion measurements (angle-of-attack and dynamic pressure) obtained from conventional differential pressure flow angle sensors at the tip of a nose-boom 1.5 fuselage diameters ahead of the aircraft body are reported. The results indicate that the radome system works well down to scale sizes slightly larger than the fuselage diameter. Finer scale measurements were found to be limited by pressure transducer response. It was learned from comparison of the power spectra determined from the conventional and from the radome angles-of-attack that the response of the radome system was superior to the conventional system due to the shorter pressure lines that were used.

Other types of pressure differential probes have been reported. For example,

19

Hermann, et al. (1984) describes an airfoil probe for angle-of-attack measurements. The results of the study showed that a small airfoil probe consisting of a small canard wing mounted appropriately on an airframe and properly tapped can serve as a viable probe for sensing angle-of-attack. An NACA 0012 airfoil section was used in wind tunnel tests. The study reported that differential pressure coefficients greater than 3 at high angles-of-attack were achieved. These coefficients are reported to be an improvement of a factor of 2-3 over comparable coefficients obtained from hemispheric probes.

In addition to the direction of the relative air velocity, the magnitude must also be measured. Computation of the magnitude of relative airspeed requires a measurement of total temperature. Total temperature is typically measured with a thermocouple or resistance temperature device (RTD). Typically, a total temperature probe is designed with the temperature sensing device situated in a volume where the air is partially stagnated, vented, and shielded to minimize radiation heat losses. For example, the NASA F-104 and the NASA ER-2 instrumented aircraft obtain total temperature measurements from a strut-mounted transducer positioned on their respective fuselages.

The quality of the total temperature measurement, however, is less important than the quality of the total and static pressure measurements, and the uncertainty in the final wind calculation is virtually independent of small errors in the total temperature measurement. Therefore, an inexpensive thermocouple generally gives sufficient performance. Insulation of the thermocouple from the fuselages is necessary to prevent the thermocouple from measuring the temperature of the aircraft instead of the air with each instrument calibration is required. Each type of instrument, however, has its own calibration problems. The following briefly summarizes the literature associated with calibration of airborne wind meaurement instruments.

Gracey and Scheithauer (1951) present results of a flight investigation of the variation of static pressure error on a static pressure tube with distance ahead of a wing and a fuselage. A discussion of the effect of distance in front of the aircraft on the error of static pressure measurement is presented for both a wing tip installation and a fuselage-nose installation.

It is reported by Haering (1990) that the airdata calibration required for measuring winds with an instrumented aircraft must be more accurate than that needed for other aircraft research programs. He reports tower fly-bys with the NASA F-104 aircraft and the use of radar acceleration-decelerations to calibrate Mach number and total temperature. The F-104 aircraft and instrumentation configuration, flight test maneuvers, data corrections, calibration techniques and resulting calibration and data repeatability are discussed. The paper concludes that the Mach number indicator could be calibrated repeatedly at $\pm$ 0.003 subsonically and $\pm$ 0.005 supersonically. Total temperature was calibrated and found to have a recovery factor of 0.986 with a $\pm$ 0.009 scatter in the data. The author recommends, from his investigation, a number of design and operation procedures for future airdata systems for aircraft used to measure winds aloft. These include (1) using a nose-boom with dual angle-of-attack and flank angle-of-attack vanes to reduce the sensitivity of upwash and sidewash on Mach number; (2) rigidly attaching the nose-boom and IRU to the same structure to minimize geometric alignment variability.

Geenen and Moulton (1991) describe a system to calibrate airdata probes at angles-of-attack between 0 and 90 degrees. The system uses a test fixture mounted to the roof of a ground vehicle which includes an onboard instrumentation and data acquisition system for measuring pressures and flow angles. The system was designed to provide convenient and inexpensive airdata probe calibrations for projects which require airdata at high angles-of-attack. The authors note that previous sub-

sonic data for the NACA standard pitot-static tube with vane type flow direction indicators was limited to 20 degrees angle-of-attack. The new type of probe introduced was tested to 90 degrees angle-of-attack in a wind tunnel and with the ground vehicle system. They also report an airdata probe with a swiveling pitot-static tube and the calibration of it with the ground vehicle system. They conclude that the swiveling-head airdata probe's larger region of total and static pressure insensitivity to angle-of-attack and angle-sideslip make it more suitable for high angle-of-attack flight than the standard NACA airdata probe.

Moes and Whitmore (1991) present preliminary results from an airdata enhancement algorithm with application to high angle-of- attack flight. The technique is developed to improve the fidelity of airdata measurements during dynamic maneuvers. The technique is reported to be particularly useful for airdata measured during flight at high angular rates and high angles-of-attack. A Kalman filter was used to combine information from research airdata, linear accelometers, angular rate gyros, and altitude gyros to determine better estimates of airdata quantities such as angle-of-attack, angle-of-sideslip, airspeed and altitude. The paper develops the state and observational equations used by the Kalman filter and shows how the state and measurement coherence matrix was determined from flight data. Flight data is used to demonstrate the results of the technique and the results are compared to an independent measurement source. Flight test data from the F-18 HARV were used to show that the Kalman filter-estimated airdata is more realistic than measured airdata during high angle-of-attack and high angular maneuvering. This has been verified using information from radar and meteorological data.

Larson and Ehernberger (1985) describe a flight test technique for controlled survey runs to determine horizontal atmospheric pressure variations and systematic altitude errors that result from space positioning measurements. The survey

22

data can be used not only for improved airdata calibration but also for atmospheric structure and space positioning accuracy performance. The authors report that data from the survey technique developed indicate that increased accuracy and improved static pressure position error calibration using radar and rawinsonde pressure measurements was achieved. In addition, the survey technique can be useful in studies of pressure gradients, atmospheric refraction and radar tracking performance.

Larson, et al. (1987) carried out flight tests with an F-14 aircraft to evaluate the use of flush pressure orifice on the nose section for obtaining airdata at transonic speeds over a large range of flow angles. The flight tests provided data to validate algorithms developed for the shuttle entry airdata system design at NASA Langley Research Center. Data were obtained for Mach numbers between 0.6-1.6 for angles-of-attack up to 26 degrees and sideslip angles up to 11 degrees. The authors conclude that with careful calibration of airdata systems with all flush orifices can provide accurate airdata information over a large range of flow angles. Several orifices on the nose cap were found to be suitable for determination of stagnation pressure. Other orifices on the nose section aft of the nose cap were shown to be suitable for determining static pressure. Pairs of orifices on the nose cap provided the most sensitive measurement for determining angles-of-attack and sideslip, although orifices located further aft on the nose section could also be used.

2.2 Inertial Measurements

Vehicle inertial attitude and velocity are typically provided by inertial navigation systems (INS) for wind measurements from aircraft borne sensors.

Ground speeds and angles, as well as Euler angles and rates, are determined from the INS. Two types of INS have been used: stable platform systems and strapped down systems. The NASA B57 Camberra and the NASA ER-2 aircraft use a stable platform system Carousel IV and Litton LTN-72RH, respectively, while

the NASA F-104 employed a strapped down, ring laser gyro. A brief description of an INS system is that the INS utilize inertial elements (i.e., accelerometers and gyros) to sense vehicle acceleration from which velocity and position can be determined. In the stable platform system these sensors are mounted on gimbaled platforms, containing at least three gimbals, which isolate them from vehicle motion and physically locate them in the desired coordinate reference frame. In local level north pointing systems, this reference frame is the local geodetic frame, and the gyro and accelerometer input axes are forced to remain as closely coincident as possible to the north, east, and vertical directions when the vehicle is in motion.

If the sensors are "strapped down" on the carriers directly, no gimbals and servo-motors are necessary. This type of INS mechanism is called a strapdown system (SDS). The accelerometer signals are measured in a body-fixed coordinate frame and transformed to a navigational reference frame by means of the gyro signals. This results in the following advantages in comparison with the stable platform systems (Lechner (1980)):

- simple mechanical construction

- the provision of accelerations and angular rates in body-fixed axes

- easy maintenance due to the modular construction
  and the economical provision of redundancy by means of skewed sensitivity axes.

However, against these advantages must be weighed certain drawbacks:

- increased demands on the efficiency of the navigation computer

- and extreme demands on the accuracy of the sensors, which have to measure the full dynamic environment of the SDS.

Regardless of which type of INS is used, it can introduce significant dynamic error into the wind vector computed from the measured ground speeds. These errors

are discussed in detail in the section on error analysis.

Considerable literature is available on INS systems. General descriptions are given in Puckett and Ramo (1959); O'Donnell (1964); and Pitman (1962).

Gorenshteyn and Shul'man (1970) describe the theoretical principles underlining inertial navigation and the basic functional elements of inertial navigation systems. General and specific representations of the algorithms for determining the running coordinates of an object are examined as applied to certain practically important methods of constructing an INS. The classification, analysis of error, preparation for operation, and also problems of protecting INS from external sources is also discussed.

Lechner, Hotop, and Zenz (1983) provide a description of the instruments and the data evaluation techniques for testing of inertial navigation systems both hardware and software. They discuss the inertial navigation system (platform systems) installed in an aircraft and how it provides signals for course and altitude. ground speed, and position determination. They note that the systems can be flight tested for various criteria: checking the system accuracy, determining its reliability, checking the aiding method for increasing the system's accuracy, obtaining knowledge as to the air behavior of an inertial systems in flight by means of the use of air models and optimal filters. They also point out that external measurement aids are available which include radar tracking systems, cinetheodolites and TACAN for exact positioning of the aircraft.

A complete description of the Carousel IV inertial navigation system used in the NASA B-57 aircraft is provided in the System Technical Description Manual, provided by the manufacturer (AC Electronics, Division of General Motors Corporation). Weber (1975) also reports on statistical studies of the accuracy of the Carousel IV inertial navigation system. Three Carousel IV inertial navigation sys-

tems were studied by Weber for accuracy during flights over the north Atlantic. Errors associated with inertial platform are also discussed by Geller (1968). Geller describes the differential equations for navigation errors of a local level and undamped inertial platform that continuously rotates in azimuth. From these, the time response equations for the vector position error produced by a constant level gyro drift error, as a function of platform rotation rate, are computed and evaluated. The paper shows that platform rotation attenuates the systems position error due to gyro bias and that this attenuation is a a nonlinear function of rotation rate.

McConnell (1966) reports on the kinematics of a three axis gimbaled system. The equations of constraint which must be satisfied during gimbal motion are studied. The phenomena of gimbal lock and gimbal flipping are considered and demonstrated for one type of vehicle motion. Curves indicating angular displacement, velocities and accelerations are computed and presented showing the need of a redundant four axis gimbal system to avoid gimbal lock.

Rhyne (1980) reports an experimental assessment made of two commercially available inertial navigation systems with regard to their inertial velocity measurement capability. This study was particularly designed for use in wind, windshear, and long wavelength atmospheric turbulence measurements. The assessment was based on 52 sets of postflight measurements of velocity (error) during a Schuler cycle (84 minutes) while the inertial navigation system was still operating but the aircraft was motionless. A maximum postflight error for the 52 cases was found to have a root mean square value of 2.82 m/s with little or no correlation of error magnitude with flight duration in the 1-6 hour range. As discussed in Section 3.2, this Schuler drift effect in the INS system has a particularly significant influence on the accuracy of the wind measurements.

Strapdown inertial navigation systems as contrasted to the plateform systems

26

are becoming more prevalent. Studies associated with error analysis in the strapdown inertial navigation systems have been reported. Shibata (1986) describes the strapdown inertial navigation error equations based on a quaternion relationship between fixed body frame and navigation (local vertical) frame for terrestrial hybrid navigation systems. Potter (1982) proposes steady-state Kaimal filters used as estimators for a strapdown INS. The report describes investigations as to the sensitivity of the steady-state Kaimal filters to inaccuracy in the filter parameters such as the dimensional stability derivatives.

Hotop (1985) describes the measuring and data analysis technique used for flight testing two Litton LTN-90 laser gyro strapdown type navigation systems. Reference data was produced by the Carousel IV. In the mean, accuracies of 1.4 km per hour maximum for position, of 1.2 m/s for velocity and of less than 0.1 degrees for angular position and azimuth were reported for the LTN-90 navigation systems.

Miller (1980) presents a description of an algorithm for attitude and navigation computations for strapdown inertial navigation systems. Also, Friedland (1978) presents a brief review of the theory of strapdown and inertial navigation systems. He shows that the error in the quaternion vector causes a scale factor error and an equivalent tilt vector error that propagates the same way as the platform tilt vector in a gimbaled system. A set of equations for error analysis are derived and interpreted in this paper.

Error equations for the Psi-angle in strapdown inertial navigation systems are provided by Weinreb and Bar-Itzhack (1978). It is proven in this paper that apart from a sign change the side angle differential equation in the error analysis of strapdown inertial navigation systems is identical to the one used in conventional gimbaled inertial navigation systems.

3.0 UNCERTAINTY ANALYSIS

The design of an instrument system requires an uncertainty analysis to quantify the affect of individual instrument uncertainties on the final wind velocity determined by combining the measured values through the reduction equations. Appendix B contains a detailed uncertainty analysis procedure. Typical magnitudes of potential uncertainties are presented graphically in Section 3.1. Other uncertainties resulting during operations and calibration problems also must be considered in a measurement of wind from an aircraft. The propagation of error from measurements inaccuracy of pressure, temperature, flow angle, angular displacement, and inertial velocity and discussed in Section 3.1. Error encountered during flight operations are described in Section 3.2.

3.1 Design Uncertainties

Figure 3.1 shows the effect of pressure and temperature measurement uncertainties on calculated airspeed. The airspeed uncertainty, which is calculated from the combination of Equations (A.2) through (A.7), is based on the assumptions that the static and total pressure measurement uncertainties are equal and that supersonic free stream flow is compressed by a normal shock wave before coming into contact with the ports used for pressure measurements.

Figure 3.1 also indicates that the minimal airspeed uncertainty is calculated from measurements made near unity Mach number. However, because pitot probes used for total and static pressure measurements are known to induce localized regions of supersonic flow, the simple one-dimensional theory used here may not be adequate for uncertainty predictions near unity Mach number. The uncertainty in the transonic airspeed calculation requires testing and indepth analysis.

Figure 3.2 shows the uncertainty in the square of the magnitude of the relative
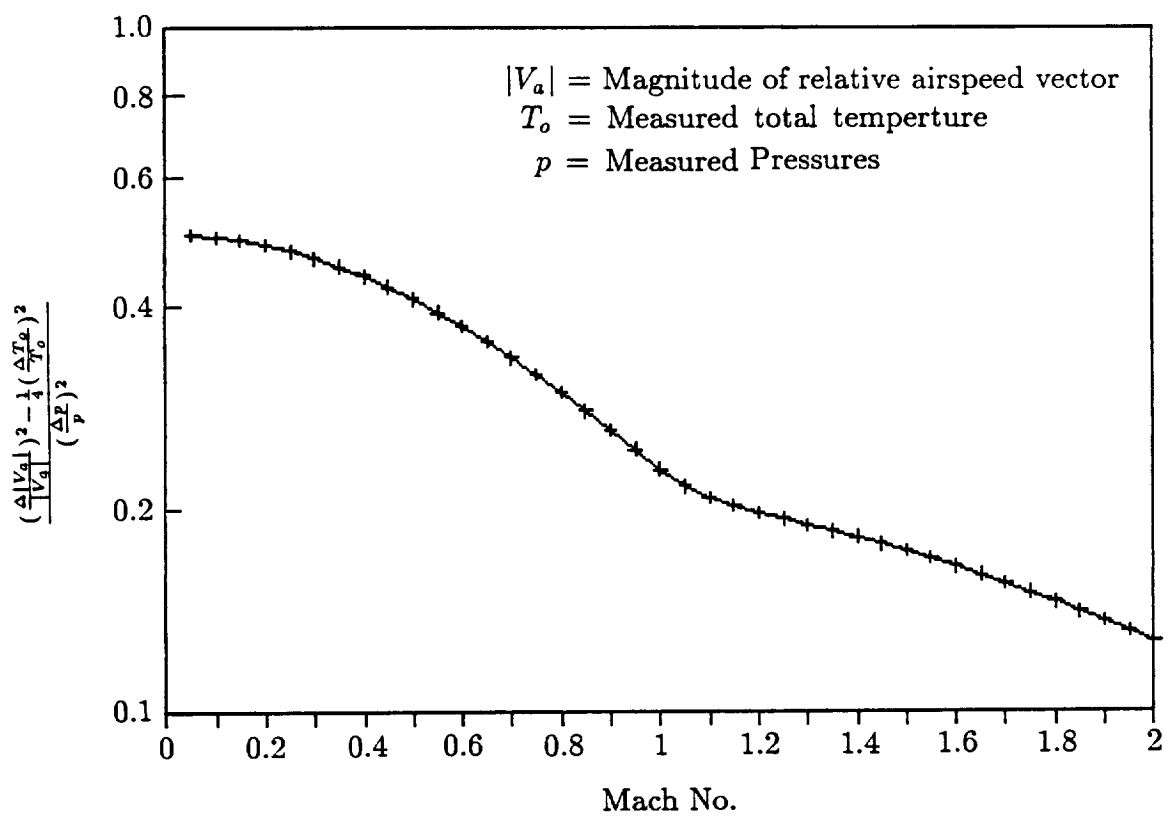
Figure 3.1 Calculated airspeed uncertainty as a function of pressure and temperature measurement uncertainties.

$|\vec{V_a}|$ = Magnitude of the error vector of
        the relative air speed

$|V_a|$ = Magnitude of airspeed vector
  α = Angle of attack
  β = Sideslip angle
  n = An arbitary power

Assumes $\Delta\alpha = \Delta\beta$

$\Delta\alpha \times 10^{-n}, Degrees$
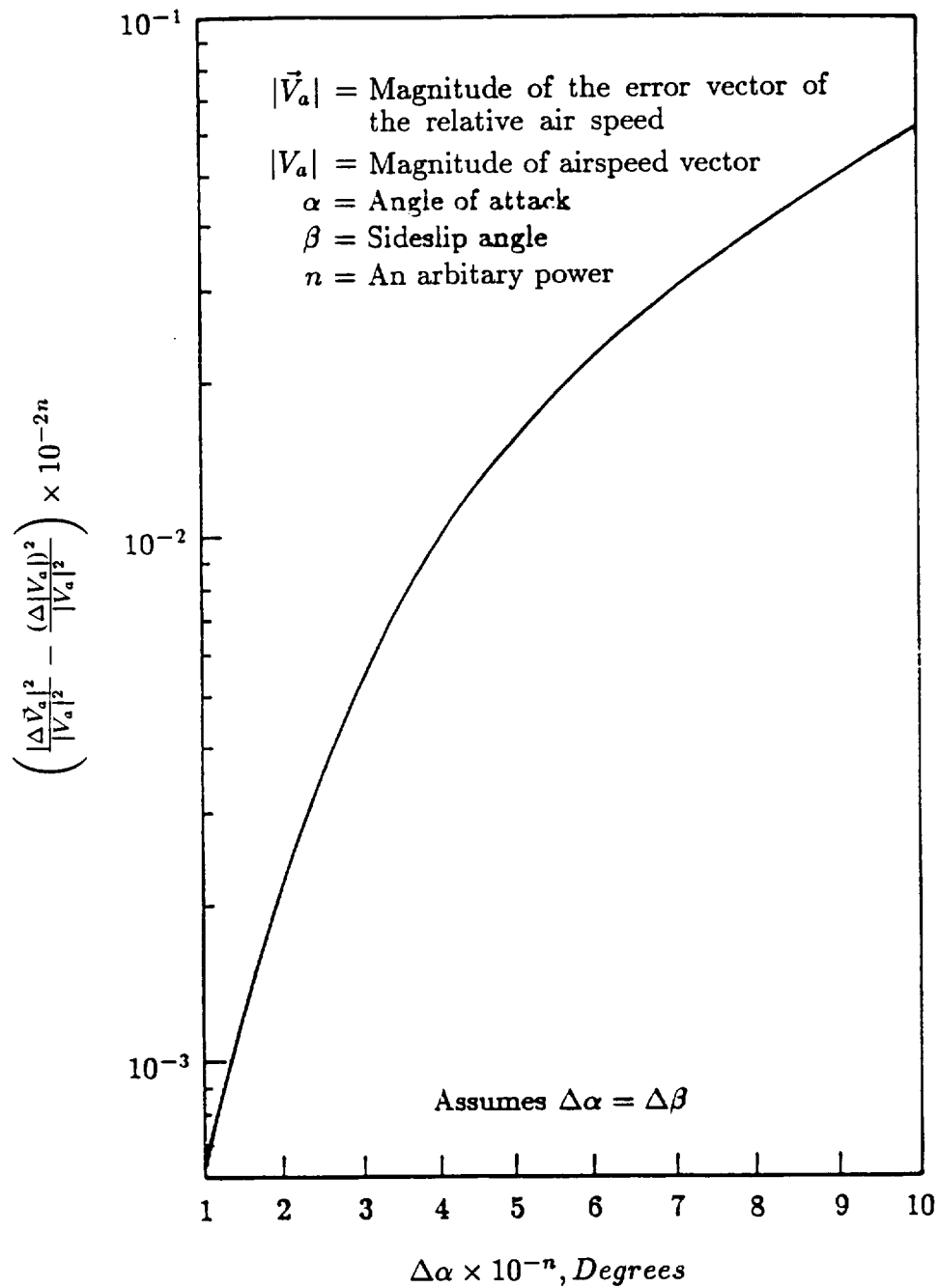
Figure 3.2 **Relative airspeed velocity uncertainty as a function of airspeed and flow angle uncertainties.**

velocity of the air vector, $|\Delta \vec{V}_a|^2$, resulting from the airspeed uncertainty and the measured flow angle uncertainty. The uncertainty in $|\Delta \vec{V}_a|$ (see Equation (A.9) is based on the assumption that the flow angles, α and β, are small ($< 5°$) and the flow angle uncertainties, $\Delta \alpha$ and $\Delta \beta$, are equal.

Figure 3.3 shows the uncertainty in the square of the magnitude of the wind velocity error vector $|\Delta \vec{W}|^2$. The uncertainty is plotted as a function of the uncertainty in the Euler angles where it is assumed $\Delta \phi = \Delta \theta = \Delta \psi$.

Figures 3.1, 3.2, and 3.3 are tools developed for a "back-of-the-envelope" determination of the wind velocity uncertainty from the uncertainties in airborne measurements. The use of these relations is illustrated by an example.

Assume that the parameters measured on an airplane have the uncertainties listed in Table 3.1.

Table 3.1   Example Measurement Uncertainties.

$\frac{\Delta p}{p}$	0.5 %
$\frac{\Delta T_o}{T_o}$	0.5 %
$\Delta \alpha, \Delta \beta$	0.1 deg.
$\Delta \phi, \Delta \theta, \Delta \Psi$	0.1 deg
$|\Delta V_e|$	1 m/s
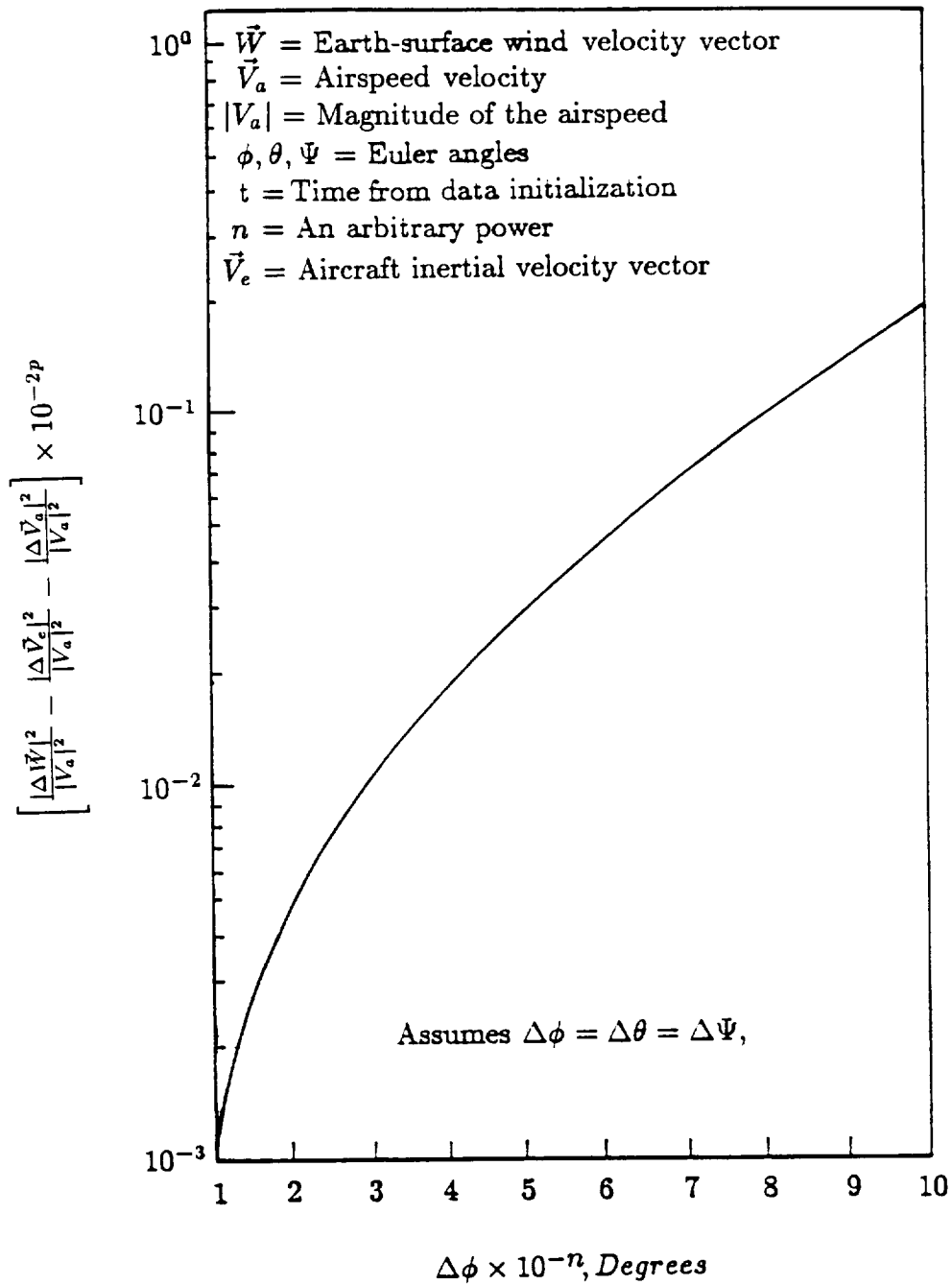
Figure 3.3 Wind velocity uncertainty as a function of relative airspeed velocity uncertainty, inertial velocity uncertainty, euler angle uncertainty, and airspeed.

32

If the airplane is flying at Mach 0.5 at sea level ($V_a \approx 345m/s$), the pressure and temperature measurement uncertainties can be used with Figure 3.1 to determine the relative airspeed uncertainty of 0.4%.

Figure 3.2 is then used to determine the effect of the angle-of-attack and sideslip angle uncertainties. For the given flow angle uncertainty of 0.1 deg., the power n on the abscissa of Figure 3.2 is set equal to -1 and the relative magnitude of the uncertainty of the relative airspeed velocity is 0.5%. Figure 3.3 is used in a similar manner, with the uncertainty in the measured Euler angles and in the inertial velocity, a relative wind velocity uncertainty of ± 2.3 m/s can be calculated. Note that no information about the direction uncertainty is contained in the figures.

3.2 Operational and Dynamic Uncertainties

Extensive investigation reported by Chang and Frost (1985); Frost, et al. (1985); Ringnes and Frost (1985); and Hill (1990) using data gathered with the Cambera B-57 aircraft has been carried out. The following draws heavily from these reports.

3.2.1 Sources of Inaccuracy in Data Reduction

Instrumentation errors influence the quantities appearing on the right-hand side of Equations 2.2, 2.3, and 2.4 and thus the accuracy of the computed wind velocities. Of these sources of instrumentation errors, the most difficult to correct is the dynamic error in the velocity inherent in the INS, termed the Schuler error to which aircraft motions contribute. All other errors can be removed by careful calibration. The effects on the magnitude of the measured wind and also turbulence calculations due to the sources of error in the instrumentation are presented next.

3.2.2 Inertial Velocity and Position Errors

The accuracy of the calculations of horizontal winds depends upon the performance of the INS and its capability to provide correct measurements of the inertial

(ground) speed of the aircraft. In recent years mechanical and electronic advances have greatly improved INS accuracy. However, a cumulative oscillation in the INS stable platform element called the Schuler drift effect, first pointed out in the famous paper by Schuler (1923), can be quite significant. Inertial navigation theory including derivation of the Schuler pendulum effects is explained in many textbooks (see for example, Boxmeyer (1964)). The Schuler error is essentially periodic with a period near that of an earth radius pendulum, 84.4 minutes. Huber and Bogers (1983) point out that a platform used in an airplane cannot strictly be kept tuned to $T_o = 84.4$ minutes after takeoff since R (distance between the airplane and center of the earth) and g (gravitational acceleration) change with altitude. They propose to define $T_o = 84.4$ minutes as the Schuler constant (for the earth). The actual period of oscillation proposed by these authors for a specific Schuler-adjusted system takes into account the gravity gradient, the mass distribution in the system, and the centrifugal forces due to the velocity of the carrying vehicle. This is called the actual oscillation period. The actual oscillation period of a specific Schuler-adjusted system (acceleration insensitive system) under specific circumstances is given by them as:

$$T = k \cdot 2\pi \sqrt{R/g}$$

where k will always have a value between 0.5 and ∞. The Schuler error behaves sinusoidally and will thus change polarity. The error caused by a slow oscillation of the INS stable platform causes the two horizontal accelerometers to detect a part of the gravity vector. This false indication of acceleration is carried through the integration for velocity and produces errors in the W_E and W_N values. Distance traveled or geographical position is obtained from a second integration of the measured accelerations. Thus the Schuler oscillations will create errors in acceleration, velocity, and position. The following procedures can be used to estimate the velocity

34

errors associated with Schuler drift.

Position error can be computed from aircraft data during overflight of landmarks where exact geographical locations are known. Since acceleration, velocity, and position errors are all interrelated, the Schuler error can experimentally be investigated by obtaining data on either one of the three parameters having a Schuler oscillation induced error. The velocity error is generally small but increases with time, e.g., after several hours of operation it can be on the order of 3 to 5 m/s (Rhyne (1980) and Lenschow (1983)). The magnitude of the position errors for the Carousel IV INS used in B-747 aircraft reported by Weber (1975) normally are on the order of 10 nautical miles or less even after transatlantic flights. These errors are not critical for pure navigation purposes. But, when the objective is to calculate wind velocity, the Schuler error can be quite important.

To illustrate the magnitude of in-flight Schuler error, data from a Flight with the NASA Cambera B-57 aircraft are presented (Frost, et al. (1987). A box pattern flight plan as shown in Figure 3.4 was flown sequentially at 1000 ft levels over Boulder, Colorado, in February 1984. Details of the flight and results are given in Chang and Frost (1985). Each time the B-57 flew the leg heading east, an event marker on the ground was activated to record the moment a north-south running road lined up perpendicular to the flight path (see Figure 3.4). INS recorded longitude at the time of the event marker can thus be compared with the known longitude of the road to construct the Schuler position error (see Figure 3.5a). The exact latitude of the aircraft at the time of the event markers is less certain. In fact, it depends upon the ability of the pilot to fly the intended flight path. But, since the flight paths were flown toward a fixed landmark, only small deviations in the latitude position of the east-west runs would occur. A similar indication of position errors has also been plotted for the latitude, Figure 3.5b. In both cases, the error
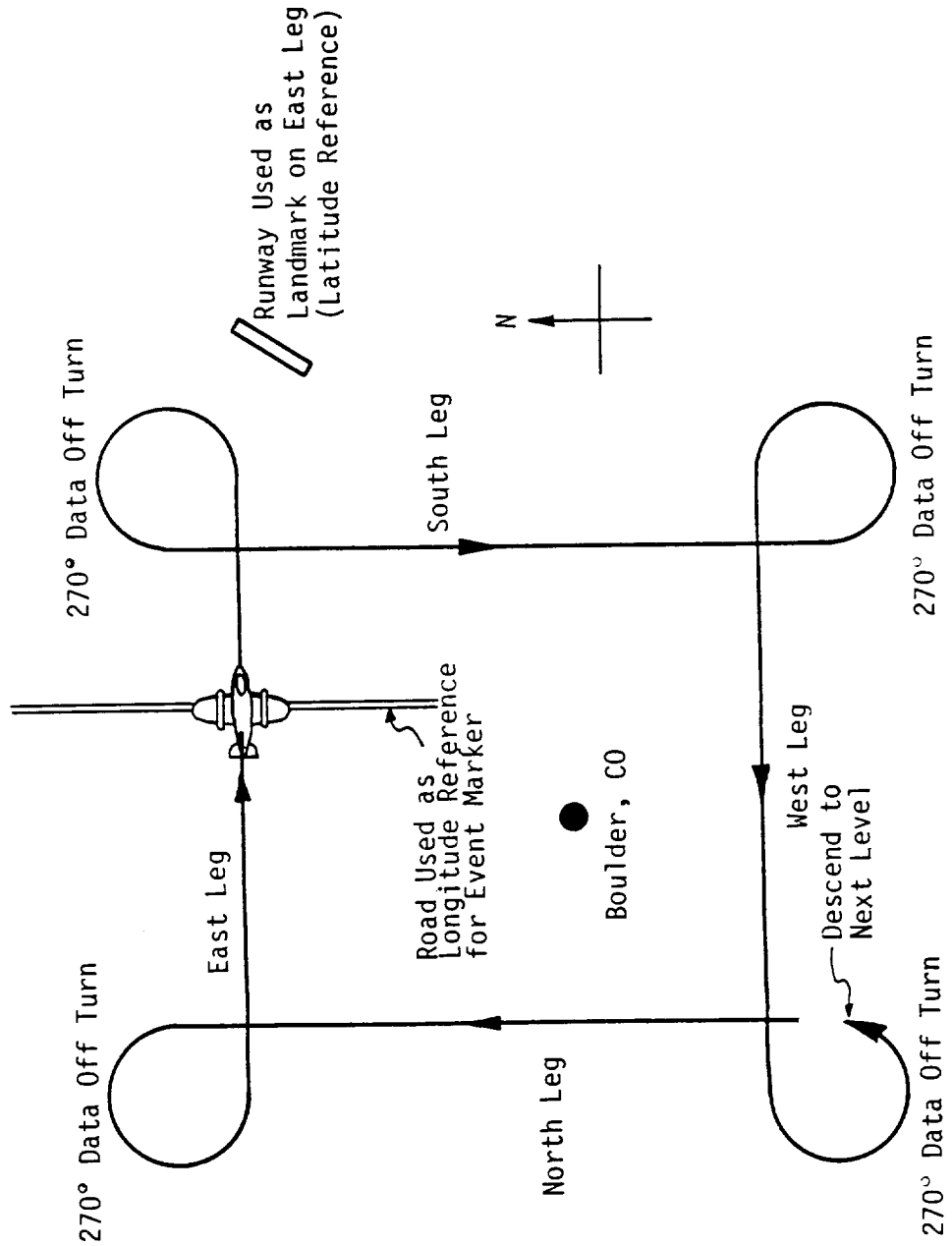
Figure 3.4 Event marker location of B-57 on box pattern flights.
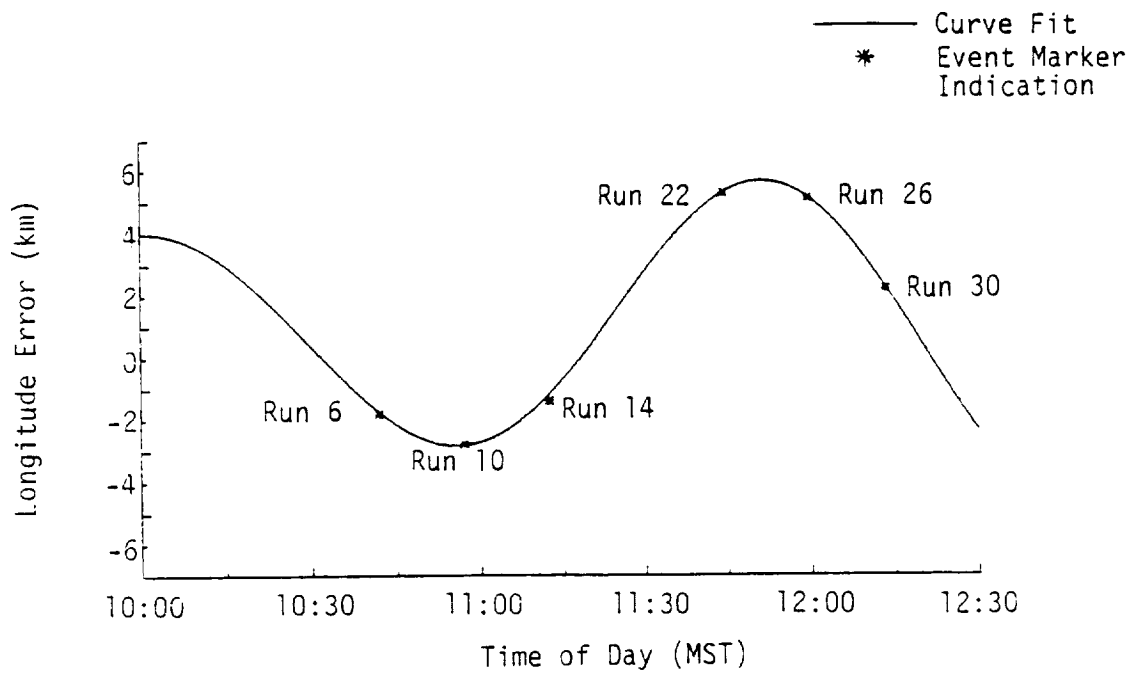
(a) Error in INS longitude indication
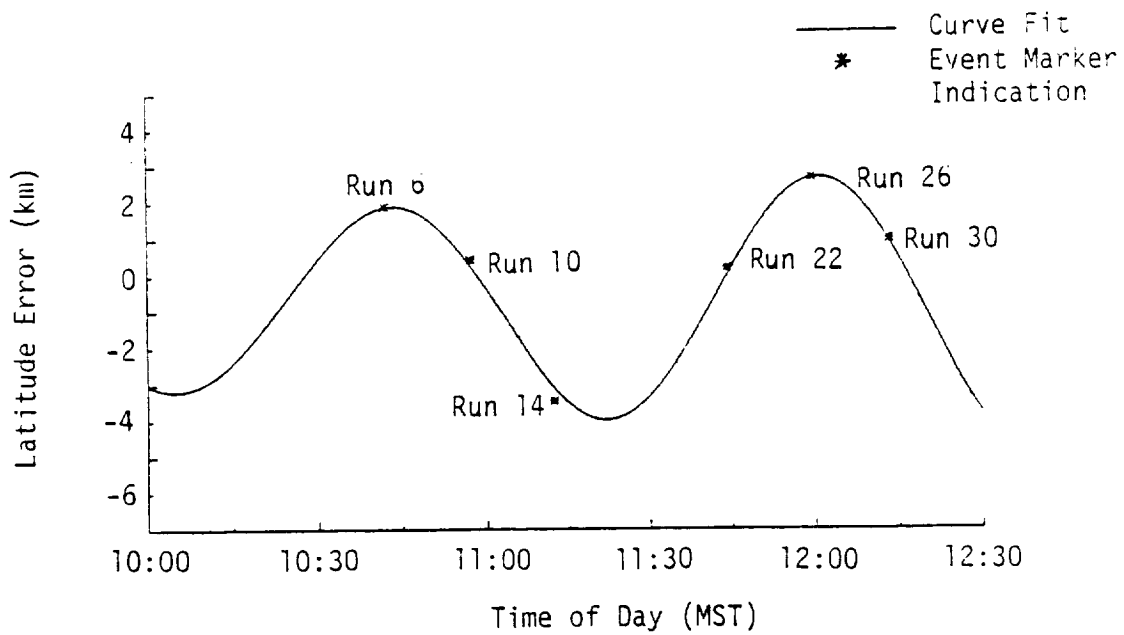
(b) Error in INS latitude indication

Figure 3.5   In-flight Schuler position error.

37

appears to have a sinusoidal behavior. A curve fit of the data suggest the latitude error has a 77-minute period of oscillation, and the longitude has an 111-minute period. The latitudinal period is reasonably close to the Schuler constant of 84 minutes, but the longitudinal period does not conform to that for the latitude.

Another flight following the same flight pattern and the same technique for marking geographical position by event markers is shown in Figure 3.6. The dashed lines outline sinusoidal trends but are not represented by mathematical equations. The latitude oscillation compares with a period of approximately 110 minutes which is similar to the previously reported longitude oscillation. The longitude error contains more scatter in the data, although the period seems to be of roughly the same length as the latitude oscillation on this flight.

The magnitude INS position errors identified are within a range of less than 15 km or 10 nautical miles. From a commercial aircraft operation standpoint, these errors are not a large problem, particularly in the proximity of an airport where other means of navigation are available. However, Schuler position errors are of significance for wind measurements. Exact ground tracks are needed to determine terrain effects on turbulence such as wake regions behind mountains, etc. An error on the order of several kilometers can drastically distort the picture.

The INS velocity errors which are related to position error can be of the same order of magnitude as the wind speed being measured. An estimate of the velocity errors are presented in Figure 3.7. The velocity error curves are calculated by taking the derivative of the position error curve fits illustrated in Figure 3.5. The influence of these errors is discussed later.

The Schuler error was further investigated with other flights. The aircraft was tracked by the NASA EPS-16 # 34 tracking radar. The radar track provided the location and the ground speed of the aircraft throughout the flight. The post-flight
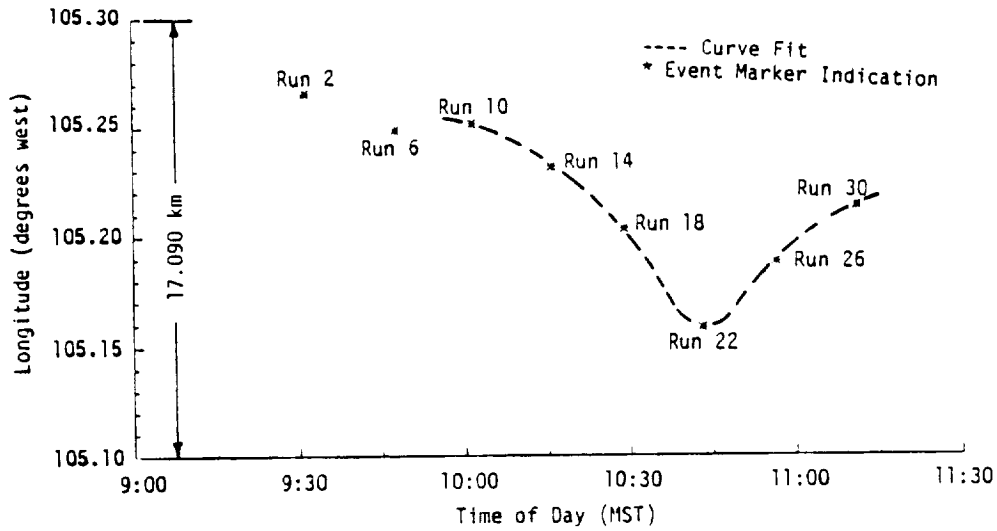
(a) Drift in INS longitude indication
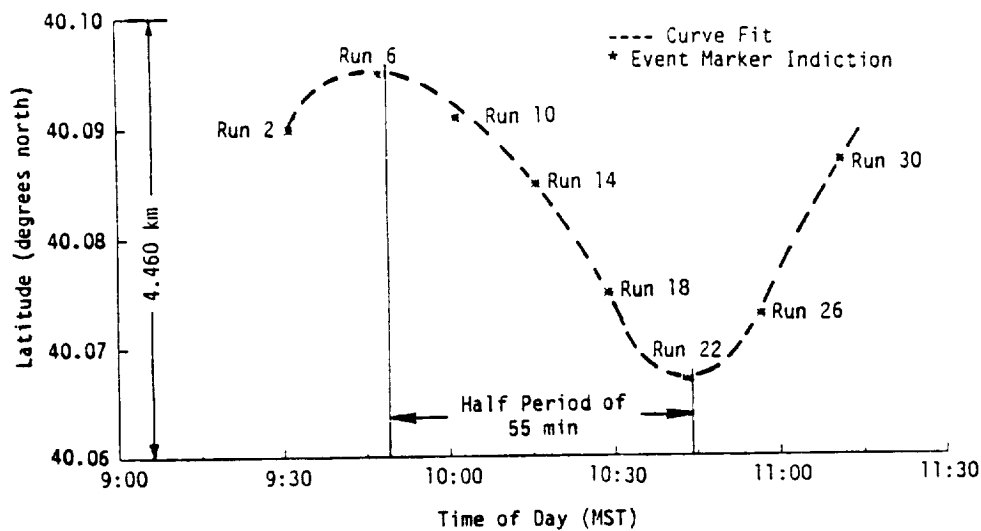
(b) Drift in INS latitude indication

Figure 3.6   In-flight Schuler position error.
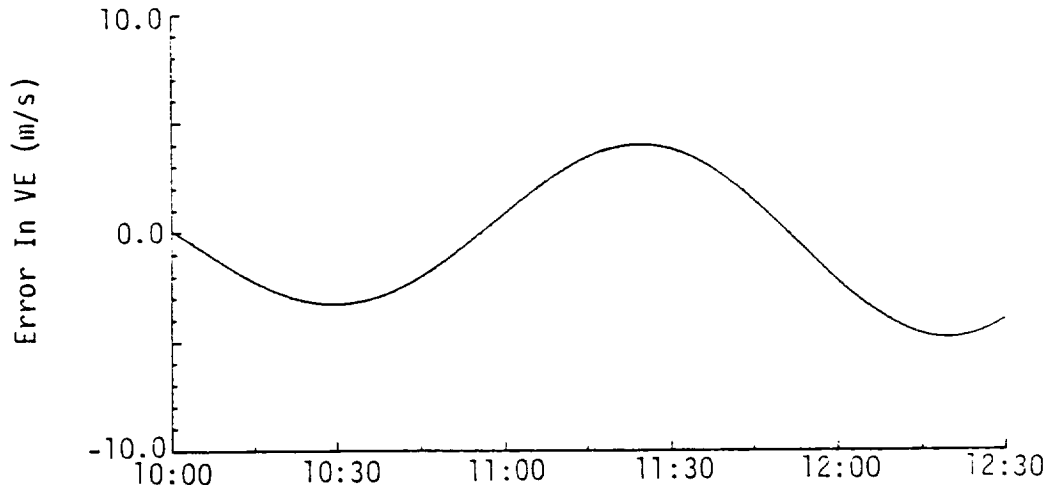
(a) East inertial speed error
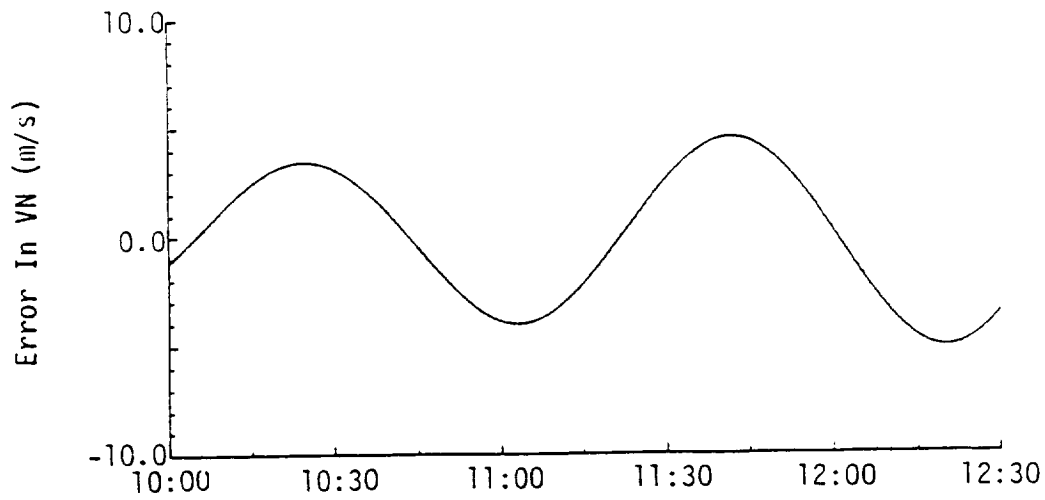
(b) North inertial speed error

Figure 3.7   In-flight Schuler inertial speed error.

Schuler velocity errors were investigated. The north-south and east-west velocity errors of the flight and the ensuing post-flight velocity measurements are plotted in Figures 3.8 and 3.9. The in-flight velocity errors are obtained by comparing aircraft and radar data assuming the radar indications are free of error. The data recorded on the ground is a direct measure of the indicated velocity from the INS while the aircraft was parked and hence not moving. This velocity fluctuation is attributed to the Schuler error. The INS was left on during the entire time span covered in the plots. Both figures show one complete cycle of a near perfect 84-minute Schuler oscillation in the post-flight data while the vehicle was parked. This is in keeping with Huber and Bogers (1983) who noted that near the ground without accelerations involved the Schuler oscillations will have an 84.4-minute period. In the first half of the flight the errors are more random in their behavior and the oscillation is irregular. This complicates attempts to model or predict the error in advance. Lenschow (1972) suggests that post-flight data recorded with a stationary aircraft be used to back out the error. He proposed to simply trace back a recorded post-flight error oscillation with an 84-minute period constant amplitude sinusoidal curve. The Frost, et al. (1987) study shows, however, that both the period and the amplitude of the velocity error are altered substantially during flight and thus the Lenschow (1972) approach would not be successful in their case. It should be noted that while the inertial velocity measurement errors strongly influence the horizontal wind vector calculations, they generally have little effect on the gust velocity computations because the effect of the slow variations in velocity is greatly diminished or eliminated when the average velocity is removed.

3.2.3 Flow Vane Errors

Ringnes and Frost (1985) observed in analyzing the B-57 data that constant differences existed between the angles of attack measured at the three different
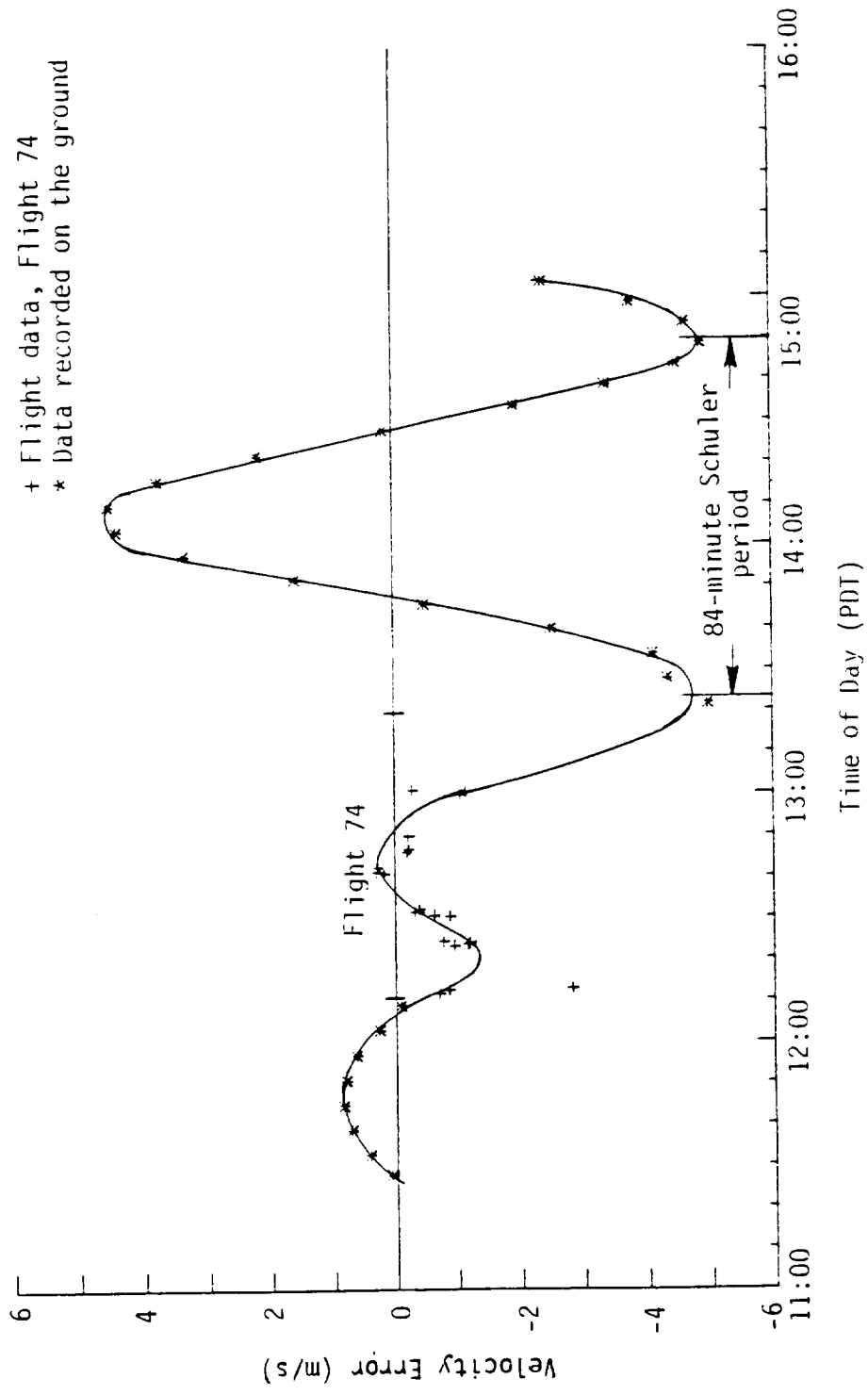
Figure 3.8   Error in east inertial speed.
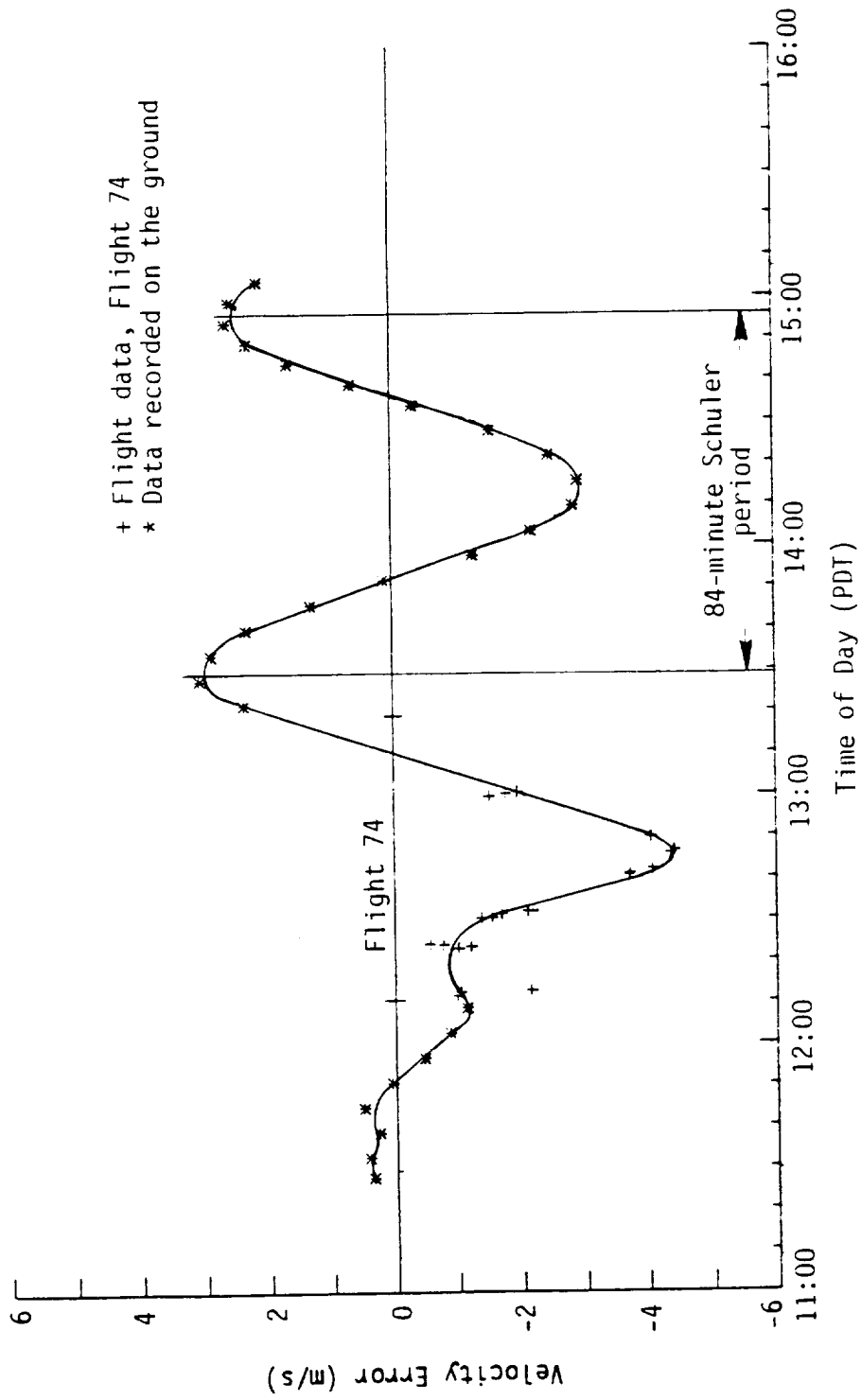
Figure 3.9 Error in north inertial speed.

43

stations along the wing. The constant offset from the true value again has little influence on the computed turbulence since the mean value is removed during the computation. The angle of attack terms have negligible effect on the computed values and therefore the inaccuracies cause no problems in the total horizontal wind vector computation. The cause of the angle-of-attack difference, however, were attributed to misalignment of the wing tip booms.

The average sideslip angles were also found to be different from the expected value. All aircraft are designed directionally stable and will fly with zero average sideslip angle unless forcefully kept in a sideslip flight condition. During one flight an average sideslip angle of 2.23 degrees was recorded. The source of the error is not clear but boom misalignment or problems with the data acquisition system were suspected causes.

3.2.4 Influence of Error Corrections

The influence the INS velocity and position, sideslip angle, and airspeed errors have on the calculation of horizontal winds is discussed next. A series of wind vectors are plotted before and after corrections have been made along the flight path recorded by the INS during given flights of the NASA Cambera B-57. Each vector represents a one-second average from the 40 samples per second data tapes.

In Figure 3.10 one of the box patterns flown on a particular flight is plotted. In this figure, no corrections have been made. There are some obvious inconsistencies in the wind vectors, particularly, at the corners where it is expected that the wind should agree closer between the two runs. The aircraft made 270-degree turns between runs which take less than two minutes. The wind direction is not expected to change significantly during that short of an interval. Instrumentation errors are, therefore, the probable cause for the discontinuities in wind direction. Figure 3.11 differs from Figure 3.10 only by removal of the 2.23-degree sideslip error in

44
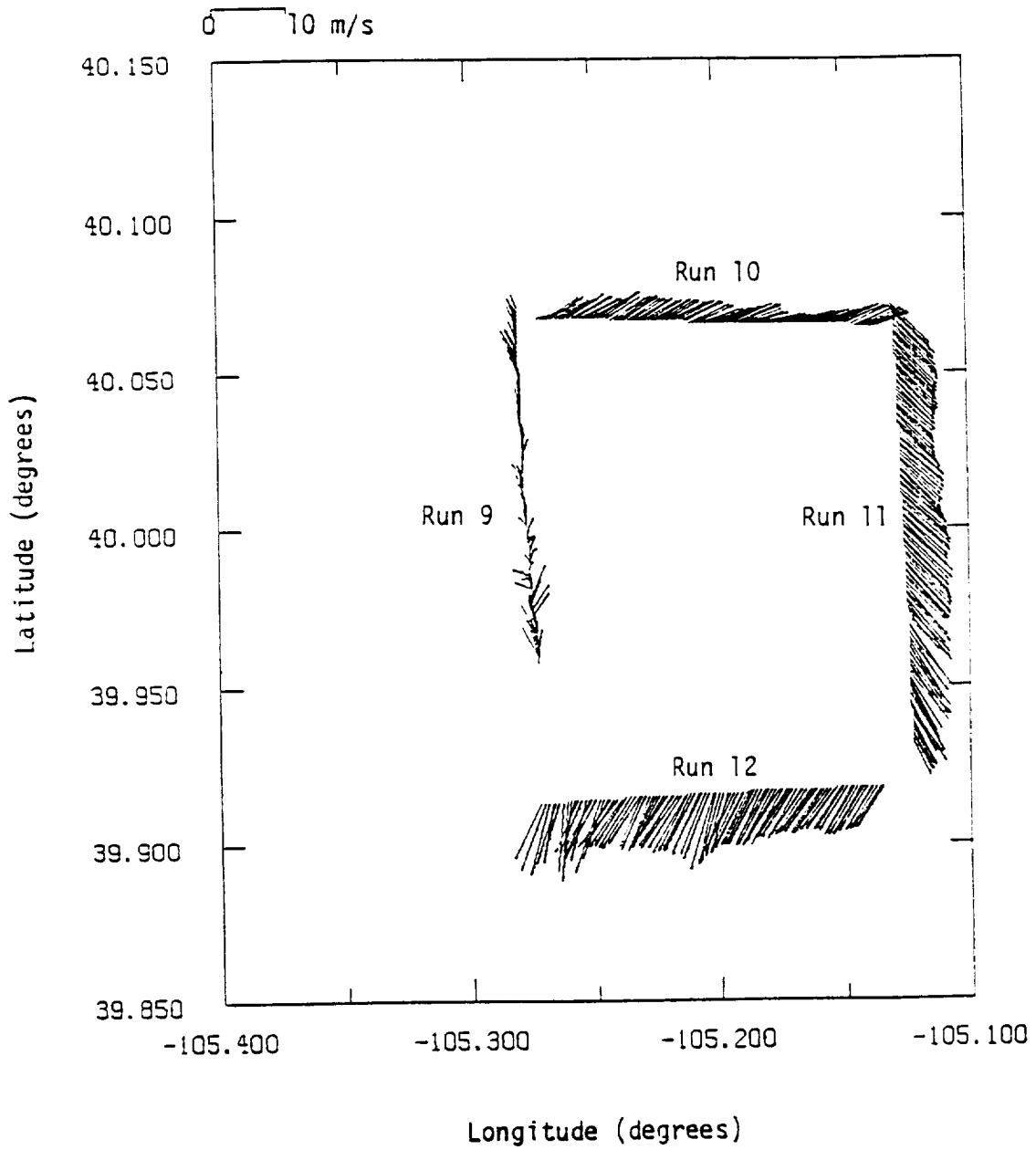
Figure 3.10   Horizontal wind vectors without corrections.

45
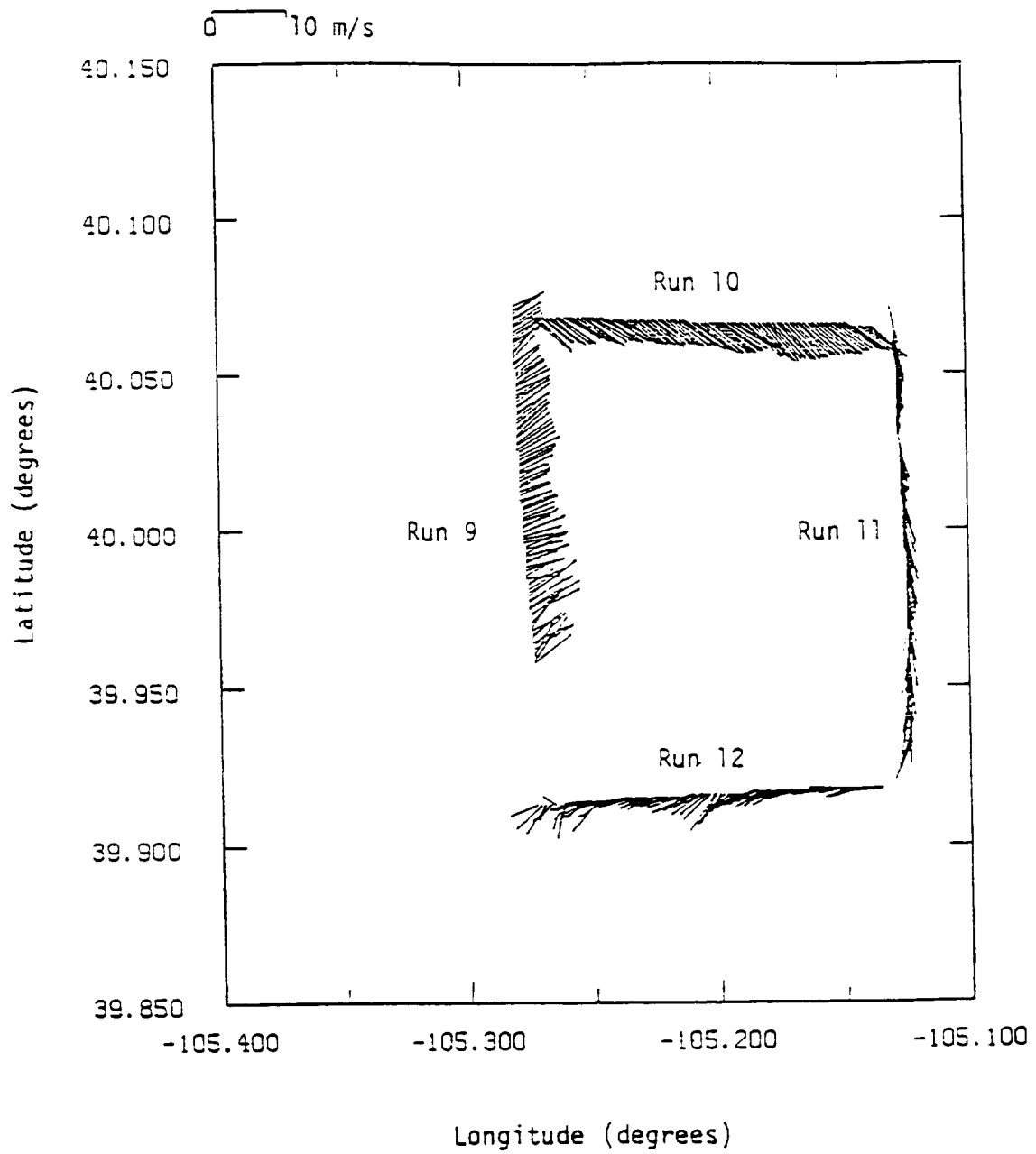
Figure 3.11 **Horizontal wind vectors with sideslip-angle corrections**

the calculation of the wind vectors. It is debatable whether this correction alone has improved the wind vectors but it clearly demonstrates that seemingly small errors have significant effect on the wind vectors. In Figure 3.12 corrections have been made for all known errors. The discontinuities in the wind vectors at the corners have all but vanished except for the bottom left-hand corner. However, as the numerical order of the runs indicates the box pattern was flown in a clockwise direction; thus, the beginning of the first leg of the run and the last are separated in time by approximately 15 minutes. Therefore, it is conceivable that the wind could have changed in that time span.

Discussion of other sources of errors and their magnitudes is given in the afore-mentioned references. These are less significant in calculating wind velocities and the interested reader should consult the references directly for more information.
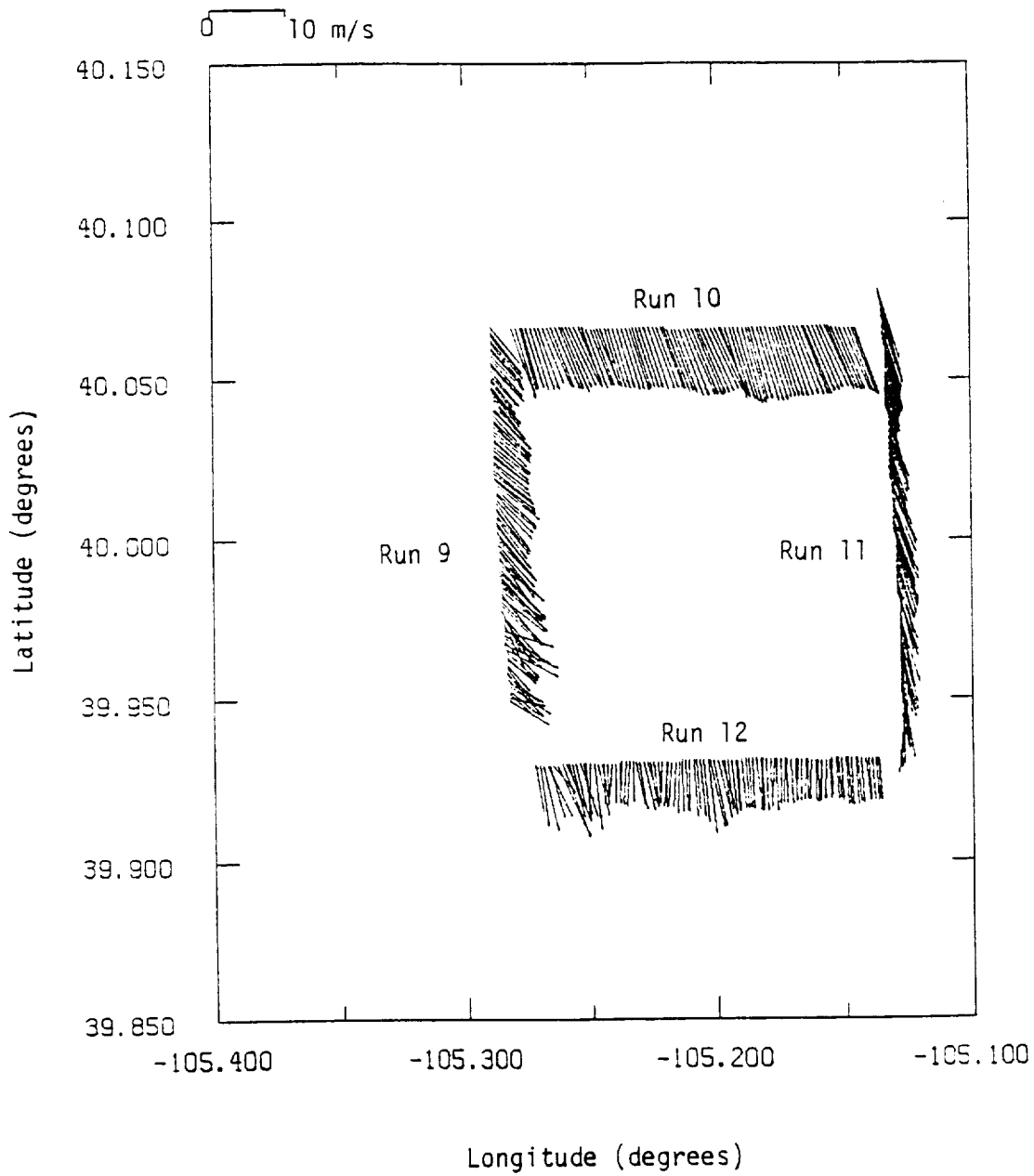
Figure 3.12   Horizontal wind vectors after airspeed, sideslip-angle and inertial velocity and position corrections.

4.0 DATA COMMUNICATION

4.1 Data Transmission

Communication of transducer data to a ground based data acquisition system is generally required for an instrumented aircraft measurement program. Therefore, telemetry techniques capable of transmitting instrumentation data to the ground-based data acquisition system are required. Although several methods are available, specifically, three telemetry methods are most promising: pulse-amplitude modulation (PAM), frequency modulation (FM-FM), and pulse-code modulation (PCM). The PCM telemetry technique is potentially the best for aircraft measurements based on cost and performance factors, which are discussed in detail in this section.

Several factors influence the choice of telemetry techniques for a specific application, including noise, filtering, and sample rate. Signals are especially susceptible to noise contamination along data transmission lines between the transducer and amplifier. Standard practices involving the use of twisted-pair wires, shielded cables, and differential-input amplifiers, can be used to minimize noise picked up by transmission wires. Since several of the specified transducers have maximum signal levels in the millivolt range, their signals must be amplified to a level compatible to the data acquisition system. If the transducer signal is amplified before the noise is introduced, the problem is greatly reduced early in the transmission path. For this reason, only transducers with integral amplifiers should be used. Integral-transducer amplifiers reduce the parts count significantly in addition to reducing noise.

Additional signal conditioning, such as filtering, is not generally required aboard the aircraft, but must be performed by the ground- based data acquisition system. The data acquisition system includes an appropriate mass storage device for later

retrieval and conditioning of the wind data. Figure 4.1 illustrates the data path aboard the aircraft.

Although the telemetry data link must introduce a minimal amount of noise, other constraints on the design are equally important with the telemetry data link. Specifically, sample rate (when applicable) and cost must be considered. The minimum tolerable sample rate of the aircraft's telemetry system is dependent on the data layer thickness and the speed of the aircraft. For a detectable layer, d, and an aircraft speed, V, the minimum sample frequency per channel is:

$$f_s = \frac{2V}{d} \tag{4.1}$$

since a minimum of two samples must be taken for a layer to be detected where V = speed of the rocket, d = minimum shear layer resolution, and f_s = sample frequency. Figure 4.2 is an example plot of required sampling frequency for an 11-channel system as a function of vertical ascent rate. This takes into account neither oversampling, which would be required with a digital filter nor the use of multiple data channels, which could be used on the aircraft. Oversampling n channels s times results in a sample frequency

$$f_s = \frac{2Vns}{d} \tag{4.2}$$

The minimum sample frequency is not a factor if an FM-FM system is used. FM-FM systems transmit a continuous signal of summed subcarrier oscillator signals which correspond to individual transducer voltage signals. The minimum detectable data layer thicknesses depend on the center frequency and modulation index of the individual subcarrier oscillators. Therefore, provided that the center frequencies are sufficiently higher than the cutoff frequencies of the corresponding transducers, no data will be lost due to frequency limitations of the telemetry system.

PAM and PCM are not continuous telemetry schemes and thus must sample no slower than the minimum sample frequency as described above. PAM is the
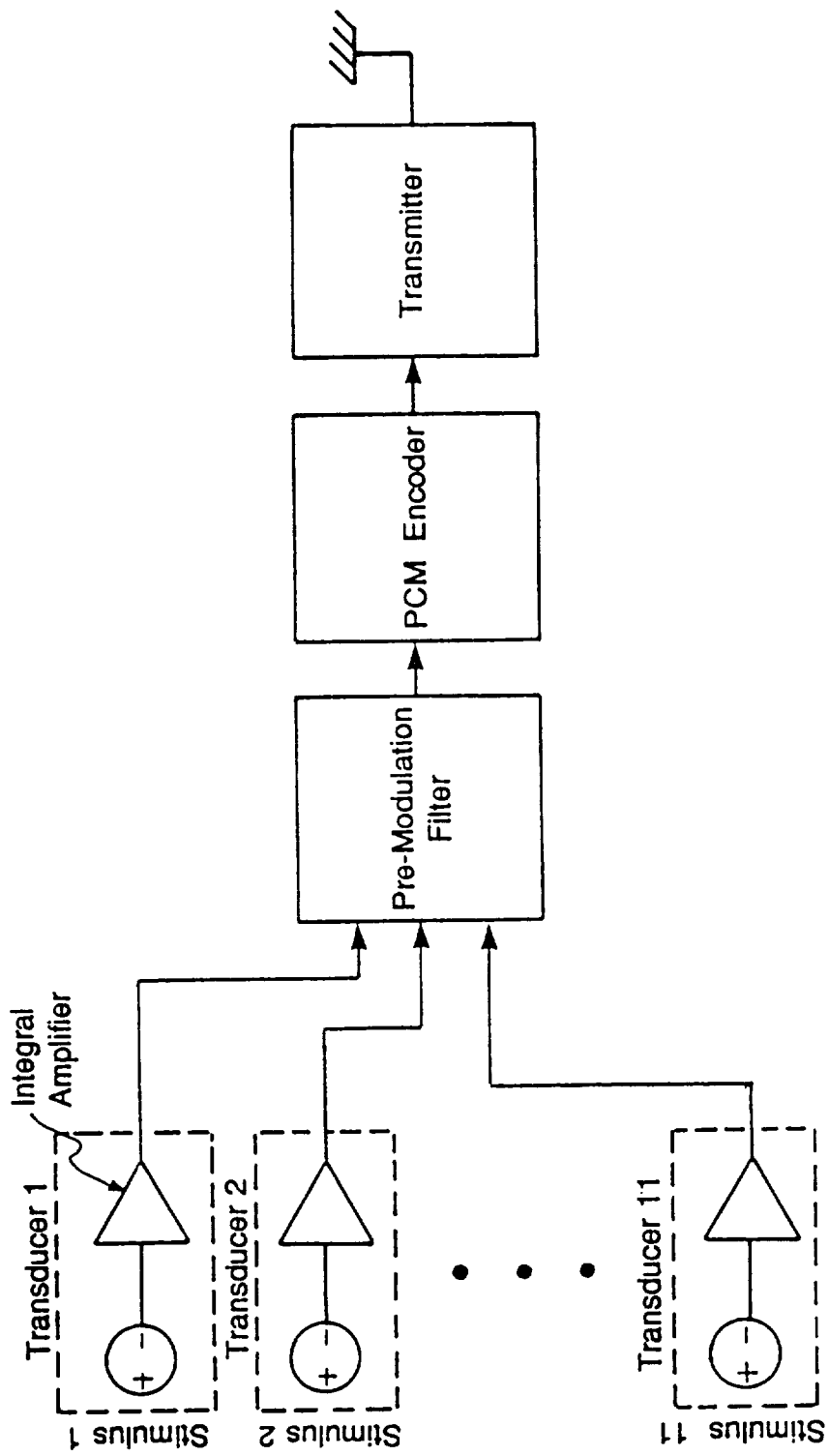
Figure 4.1 Data path aboard aircraft.
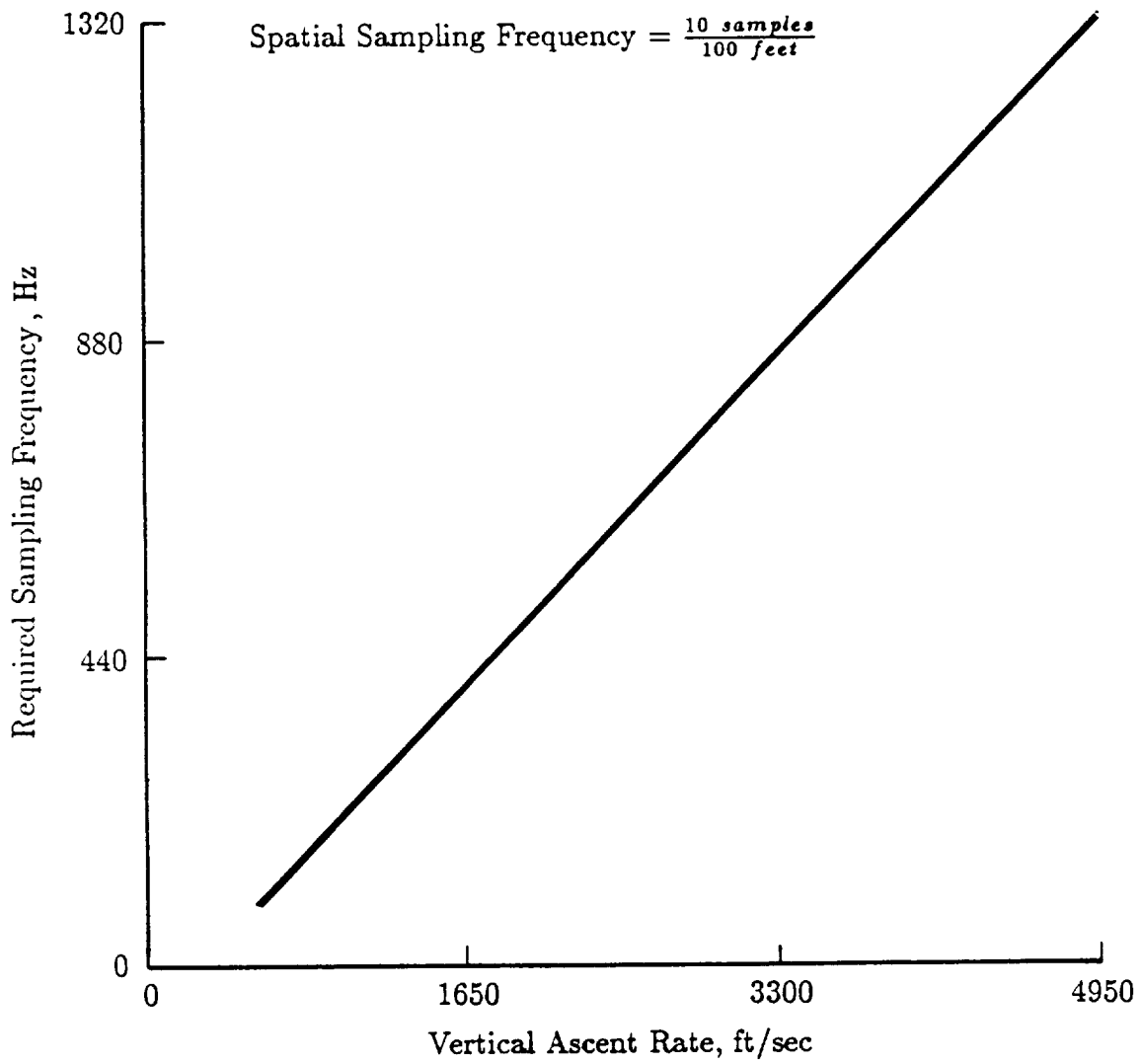
Figure 4.2 Minimum sampling frequency for 11-channel system.

simplest method of time-division multiplexing: the separate transducer outputs are sequentially switched to a common output which forms a composite waveform of the individual channels' outputs. The period of the waveform is equal to the sample interval of one channel times the total number of channels in the system. PCM operates similarly, with the exception that data is converted from analog signals to digital signals. Current sample rates of PAM and PCM encoders are up to 200,000 samples/sec and 3.2 megabits/sec respectively.

Crosstalk, gain and offset errors, and incidental frequency modulation are sources of error in data transmission. Of the three telemetry methods considered, PAM has the poorest absolute accuracy specification: typical errors between 2% and 5% of full scale can be expected. FM-FM system accuracy, as well as that of the other two methods, is highly dependent upon proper setup of the transducer output gain and offset. Depending on how close to launch time the transducer calibration is made, errors of 1% to 4% can be expected from an FM-FM telemetry system. If proper setup is obtained with a PCM system, the error induced by this system will be one least-significant bit (LSB) since the data is converted to a digital form. For an 8-bit telemetry system, one LSB equals one part in 2^8; or about 0.4%.

The recommended telemetry technique is the PCM system, based on reasonable cost, sufficient sample rate, and superior accuracy to the other methods of telemetry. This type of system allows more flexibility with the number of data channels transmitted than the FM-FM system since the latter will require additional capital expenditures for each additional channel transmitted. Additionally, the worst-case error of the final data will be due primarily to the transducers instead of the telemetry system as would be the case with PAM. Table 4.1 summarizes the characteristics of the three telemetry methods.

Table 4.1 Telemetry comparison.

Telemetry Method	Data Channel Capacity	Availability	Accuracy	Cost
PAM	Low	Low	Low	Low
FM-FM	Low	Moderate	Moderate	High
PCM	High	High	High	Moderate

Other necessary components of an onboard telemetry data link are the transmission antennas and the transmitter. Three blade antennas mounted on the rocket will transmit the telemetry signal adequately in all directions. The transmitter can be adjusted to broadcast a selected frequency which must correspond to the frequency of the receiver on the ground. This flexibility in transmission frequency could prove to be beneficial in regard to the frequency allocation and certification by the National Telecommunications and Information Administration (NTIA) upon review by the Spectrum Planning Subcommittee (SPS). The transmission frequency will typically be in the L or S band in the radio frequency spectrum.

4.2 Data Acquisition

A ground based data acquisition system is required for storing and processing the telemetered wind parameter data. An appropriate system is described next. A ground station consisting of a telemetry reception, data acquisition, and data processing system will produce all desired atmospheric profile data, store historical atmospheric profiles for future profile predictions, and permit portability to various sites.

The choice of data acquisition system is dependent on the type of telemetry system aboard the aircraft. Even though the transmitter and receiver remain the same for all types of telemetry considered, the way in which the signal is decoded to provide data from all channels is determined by the format used to transform the data signal to a telemetry signal. Since PCM is recommended as the optimum telemetry scheme for most applications, a data acquisition system compatible with PCM is discussed.

The fundamental components of a PCM data acquisition system consist of the following:

1. a PCM bit decoder to translate the frequency-modulated radio signal into a digital pulse stream,

2. a data decommutator to separate the digital signal into individual channel signals,

3. a digital-to-analog converter to transform the digital channel data into analog data, and

4. a serial time-code reader to provide time correlation with the acquired data.

In addition to these requirements, other features that will greatly benefit system quality will be incorporated. These include adaptability to a range of PCM codes, digital and analog mass storage capability, real-time display of multiple channel signals, and scaling and manipulation of these channels into desired engineering-unit parameters. These features will be incorporated into a user-friendly, stand-alone system, and will result in a highly versatile telemetry system.

Turn-key telemetry data acquisition systems are available which will accommodate all requirements for aircrafts data system. One particular system includes both the hardware and the software which obtains telemetry data. In addition to

fulfilling all of the cited requirements, the system provides data record archiving and editing capability, 16 channels of real-time analog output, user-programmable display formatting, and various scaling and look-up table capabilities. This system is available as a retrofit to a dedicated IBM PC/AT compatible or as a rackmountable 80386 system with a 100 megabyte hard disk drive. The latter option is viewed as being the more advantageous one since the data acquisition system may be installed in a single rack with the ground station receiver and a multi-channel analog tape machine used as a back-up data storage device.

5.0 SUMMARY

A review of salient features associated with measuring winds from aircraft has been given. Included is a discussion of the typical instruments and systems, the equations for reducing aircraft measurement to winds in the earth coordinates system, error analysis for assessing the accuracy of instrumentation, as well as, procedures for correcting and calibrating for errors associated with flight operations and an overview of methods for communicating measurements from the aircraft to ground station for data processing. Throughout the report a summary of the literature pertaining to various techniques available for measuring winds including some of the measurement programs for which instrumented aircraft have been developed and employed is provided. A discussion of the various types of instrumentation that have been used in previous programs, the reported potential errors and methods of correcting and calibrating the instruments and the problems associated with obtaining accurate ground speed values from INS systems is given.

The report provides a guide to researchers in the process of developing instrumented aircraft for measurement of atmospheric phenomena.

6.0 REFERENCES

An Introduction to Inertial Navigation, Litton Guidance & Control Systems brochure, Woodland Hills, CA.

Axford, D.N. (1968): "On the Accuracy of the Wind Measurements Using and Inertial Platform in an Aircraft, and an Example of a Measurement of the Vertical Mesostructure of the Atmosphere.", Journal of Applied Meteorology, Vol. 7:645-666.

Barna, P.S., and G.R. Crossman (1976): "Experimental Studies on the Aerodynamic Performance and Dynamic Response of Flow Direction Sensing Vanes", NASA CR-2683, May.

Benjamin, S.G. (1989): "An Isentropic Meso α-Scale Analysis System and Its Sensitivity to Aircraft and Surface Observations", Monthly Weather Review, Vol. 117, pp. 1586- 1603.

Bjarke, L.J., and L.J. Ehernberger (1989): "An In-Flight Technique for Wind Measurement in Support of the Space Shuttle Program". NASA TM-4154, November.

Boxmeyer, C. (1964): Inertial Navigation Systems, McGraw- Hill Book Co., New York, NY.

Brown, E.N., C.A. Friehe, and D.H. Lenschow (1983): "The Use of Pressure Fluctuations on the Nose of an Aircraft for Measuring Air Motion", Journal of Climate and Applied Meteorology, Vol. 22, pp. 171-180, January.

Brown, W.J., Jr., J.D. McFadden, H.J. Mason, Jr., and C.W. Travis (1974): "Analysis of the Research Flight Facility Gust Probe System", Journal of Applied Meteorology, Vol. 13, No. 1, pp. 156-167, February.

Bryer, D.W., and R.C. Pankhurst (1971): Pressure-probe Methods for Determining Wind Speed and Flow Direction, Her Majesty's Stationary Office, London.

Chang, H.P., and W. Frost (1985): "NASA B-57B Orographic Data Reduction and Analysis Relative to PBL Parameterization Models." Final report for NASA Goddard Space Flight Center under Contract NAS5-28558.

Crooks, W.M., F.M. Hoblit, D.T. Prophet, et al. (1967): "Project HICAT An Investigtion of High Altitude Clear Air Turbulence", Air Force Flight Dynamics Laboratory, Wright-Patterson ARB, OH, Volume 1, Report AFFDL-TR-67-123.

Davis, R.E., R.A. Champine, and L.J. Ehernberger (1979): "Meteorological and Opertional Aspects of 46 Clear Air Turbulence Sampling Missions with an Instrumented B-57B Aircraft, Volume I - Program Study", prepared for NASA Langley Research Center, NASA TM-80044.

Dutton, J.A., and D.H. Lenschow (1962): "An Airborne Measuring System for Micrometeorological Studies", <u>Studies of the Three-Dimensional Structure of the Planetary Boundary Layer</u>, Sec. 5, Dept. of Meteor, Univ. of Wisconsin, Final Report Contract DA-36-039-SC-80282, USAEPG, Ft. Huachuca, AZ.

Etkin, B. (1972): <u>Dynamics of Atmospheric Flight</u>, John Wiley & Sons, New York.

Fisher, B.D., G.L. Keyser, Jr., P.L. Deal, M.E. Thomas, and F.L. Pitts (1980): "Storm Hazards '79 – F-106B Operations Summary", NASA TM-81779.

Fisher, B.D., G.L. Keyser, Jr., and P.L. Deal (1982): "Lightning Attachment Patterns and Flight Conditions for Storm Hazards '80", NASA TP-2087.

Friedland, B. (1978): "Analysis Strapdown Navigation Using Quaternions", IEEE Transactions on Aerospace and Electronic Systems, Vol. AES-14, No. 5, pp. 764-768, September.

Frost, W., M.C. Lin, H.P. Chang, and E.A. Ringnes (1985): "Analysis of Data from NASA B-57B Gust Gradient Program." Final report for NASA Marshall Space Flight Center under Contracts NAS8- 36177 and NAS8-35347.

Frost, W. to C.K. Hill. "Action Item from NASA Dryden Meeting, May 14, 1987." FWG Associates Memorandum, dated 20-May-87, with revision 21-Aug-87.

Frost, W., H.P. Chang, and E.A. Ringnes (1987): "Analyses and Assessments of Spanwise Gust Gradient Data from NASA B-57B Aircraft", NASA Langley Research Center, Final Report Contract NAS1-17989.

Gage, K.S., and G.D. Nastrom (1986): "Theoretical Interpretation of Atmospheric Wavenumber Spectra of Wind and Temperature Observed by Commercial Aircraft During GASP", <u>Journal of the Atmospheric Sciences</u>, Vol. 43, No. 7, pp. 729-740.

Gamo, M., et al., (1975): "Observed Characteristics of the Standard Deviation of the Vertical Wind Velocity in Upper Part of the Atmospheric Boundary Layer", <u>J. Meteor. Soc.</u>, Japan, 53.

Gamo, M., et al., (1976): "Structure of the Atmospheric Boundary Layer Derived from Airborne Measurements of the Energy Dissipation Rate ϵ", <u>J. Meteor. Soc.</u>, Japan, 54.

Ganzer, V.M., R.G. Joppa, and G. van der Wees (1977): "Analysis of Low Altitude Atmospheric Turbulence Data Measured in Flight", prepared by the University of Washington for NASA Ames Research Center, NASA CR-2886.

Geenen, R.J., and B.J. Moulton (1991): "A System for Testing Airdata Probes at High Angles of Attack Using a Ground Vehicle", AIAA-91-0088, 29th Aerospace Sciences Meeting, Reno, NV, January 7-10.

Geller, E.S. (1968): "Inertial System Platform Rotation", IEEE Transactions on Aerospace and Electronic Systems, Vol. AES-4, No. 4, pp. 557-568, July.

Gorenshteyn, I.A., and I.A. Shul'man (1970): "Inertial Navigation Systems", DTIC Technical Report FTD-HC-23-327-71, January.

Gosink, J. (1982): "Measurements of Katabatic Winds Between Dome C and Dumont d'Urville", Pure Appl. Geophys., Vol. 120, pp. 503-526.

Gracey, W., and E.F. Scheithauer (1951): "Flight Investigation of the Variation of Static-Pressure Error of a Static-Pressure Tube with Distance Ahead of a Wing and a Fuselage", National Advisory Committee for Aeronautics TN-2311, March.

Gracey, W. (1958): "Summary of Methods of Measuring Angle of Attack on Aircraft", National Advisory Committee for Aeronautics TN-4351, August.

Gracey, W. (1981): Measurement of Aircraft Speed and Altitude, John Wiley & Sons.

Hacker, J.M., and P. Schwerdtfeger (1988): "The FIAMS Research Aircraft", System Description FIAMS Technical Report 8, Flinders Institute for Atmospheric and Marine Sciences, Flinders University of South Australia, Bedford Park, S.A., 5042.

Haering, E.A., Jr. (1990): "Airdata Calibration of a High-Performance Aircraft for Measuring Atmospheric Wind Profiles", NASA TM-101714, January.

Hatley, C.M. (1989): "Prelaunch Wind Monitoring Via Aircraft." CR S33450D, SIR Presentation at Johnson Space Center, Houston, Texas, November 14.

Hermann, P.J., D.B. Finley, S.C. Rehfeldt, and L.C. Benishek (1984): "Airfoil Probe for Angle-of-Attack Measurement", Journal of Aircraft, Vol. 21, No. 1, pp. 87, January.

Hill, C.K. (1990): "Feasibility of Measuring Prelaunch Wind Profiles in Support of STS Operations with an Instrumented Aircraft", PhD. Dissertation, The University of Tennessee, Knoxville, TN, May.

Hillje, E.R. and D.E. Tymms (1980): "The Ascent Air Data System for the Space Shuttle", AIAA Paper 80-0422, March.

Hillje, E.R. and R.L. Nelson (1981): "Post Flight Analysis of the Space Shuttle Ascent Air Data System", AIAA Paper 81-2457, November.

Hillje, E.R., and R.L. Nelson (1990): "Ascent Air Data System Results From the Space Shuttle Flight Test Program", NASA-Lyndon B. Johnson Space Center, Houston, TX. Personal communications.

Hotop, H.J. (1985): "Flight Testing the Litton LTN 90 Laser Gryo Strapdown System for Civil Aviation", European Space Agency, ESA- TT-904, March.

Huber, C., and W.J. Bogers (1983): "The Schuler Principle: A Discussion of Some Facts and Misconceptions", EUT Research Report 83-E-136 (ISBN 90-6144-136-6), Eindhoven University of Technology, Dept. of Electrical Engineering, Eindhoven, The Netherlands, May.

Jacobsen, R.A. (1977): "Hot-Wire Anemometry for In-Flight Measurement of Aircraft Wake Vortices", DISA Information, 21, pp. 21-27.

Karakashev, V.A. (1972): "Use if External Information on the Linear Velocity of a Vehicle for Correcting Inertial Navigation Systems", NTIS, Springfield, VA, Report No. JPRS 57282, October 17.

Kraus, H., J.M. Hacker, and J. Hartmann (1990): "An Observational Aircraft-Based Study of Sea-Breeze Frontogenesis", Boundvary-Layer Meteorology, Vol. 53, pp. 223-265.

Larson, T.J., and L.J. Ehernberger (1985): "A Constant Altitude Flight Survey Method for Mapping Atmospheric Ambient Pressures and Systematic Radar Errors", NASA TM-86733, June.

Larson, T.J., S.A. Whitmore, L.J. Ehernberger, J.B. Johnson, and P.M. Siemers, III (1987): "Qualitative Evaluation of a Flush Air Data System at Transonic Speeds and High Angles of Attack", NASA Technical Paper 2716, April.

Lechner, W., H.J. Hotop, and H.P. Zenz (1983): "Flight Testing of Inertial Navigation Systems - Hardware and Software Description", European Space Agency, ESA-TT-772, March.

Lenschow, D.H. (1965): "Airborne Measurements of Atmospheric Boundary Layer Structure", Studies of the Effects of Variations in Boundary Conditions on the Atmospheric Boundry Layer, Sec. 4, Dept. of Meteor, Univ. of Wisconsin, Final Report Contract DA-36-039-AMC-00878(E), USAERDA, Ft. Huachuca, AZ.

Lenchow, D.H., and W.B. Johnson, Jr. (1968): "Concurrent Airplane and Balloon Measurements of Atmospheric Boundary-Layer Structure over a Forest", Journal of Applied Meteorology, Vol. 7, No. 1, pp. 79-89.

Lenschow, D.H. (1971): "Vanes for Sensing Incidence Angles of the Air from an Aircraft", Journal of Applied Meteorology, Vol. 10, pp. 1339-1343, December.

Lenschow, D.H. (1972): "The Measurement of Air Velocity and Temperature Using the NCAR Buffalo Aircraft Measuring System." NCAR-TN/EDD-74.

Lenschow, D.H., and N.D. Kelley (1975): "Atmospheric Mesoscale Measurements from Aircraft", 3rd Symposium on Meteorological Observations and Instrumentation, The National Center for Atmospheric Research, Boulder, CO.

Lenschow, D.H., C.A. Cullian, R.B. Friesen, and E.N. Brown (1978): "The Status of Air Motion Measurements on NCAR Aircraft", 4th Symposium on Meteorological Observations and Instrumentation, April 10-14, American Meteorological Society, Boston, MA.

Lenschow, D.H., C.A. Friehe, and J.C. LaRue (1978): "The Development of an Airborne Hot-Wire Anemometer System", 4th Symposium on Meteorological Observations and Instrumentation, American Meteorological Society, Boston, MA.

Lenschow, D.H. (1983): "Aircraft Measurements in the Boundary Layer", A Chapter in Probing the Atmospheric Boundary Layer, originally prepared for the AMS Short Course on Instruments and Techniques for Probing the Atmospheric Boundary Layer, August 8-12, Boulder, CO.

Lenschow, D.H., X.S. Li, C.J. Zhu, and B.B. Stankov (1987): "The Stably Stratified Boundary Layer Over The Great Plains", Boundary-Layer Meteorology, Vol. 42, pp. 95-121.

Lesher, C. (1990): Personal communication with T.S. Paige. Orbital Science Corporation, Chandler, AZ.

Luers, J.K., and C.D. MacArthur (1972): "Ultimate Wind Sensing Capabilities of the Jimsphere and Other Rising Balloon Systems." NASA CR-2048, June.

MacPherson, J.I. (1973): "A description of the NAE T-33 Turbulence Research Aircraft, Instrumentation, and Data Analysis", DME/NAE Quarterly Bulletin No. 1972(4), Ottawa.

McBean, G.A., and J.I. MacPherson (1976): "Velocity and Scalar Statistics", Boundary Layer Meteorology, Vol. 10, pp. 181-197.

McConnell, K.G. (1966): "Kinematics of a Three-Axis Gimbal System", proceedings of the Third Southeastern Conference on Theoretical and Applied Mechanics, University of South Carolina, Vol. 3, March 31-April 1.

McFadden, J.D., C.W. Travis, R.E. Gilmer, and R.E. McGavin (1970): "Water Vapor Flux Measurements from ESSA Aircraft", Preprints Symp. Tropical Meteorology, Honolulu, Amer. Meteor. Soc., BIII, 1-6.

Meissner, C.W., Jr. (1976): "A Flight Instrumentation System for Acquisition of Atmospheric Turbulence Data", prepared for NASA Langley Research Center, NASA TN D-8314.

Miller, R.B. (1982): "Strapdown Inertial Navigation Systems: An Algorithm for Attitude and Navigation Computations", Department of Defence, Melbourne, Victoria, Australia.

Moes, T.R., and S.A. Whitmore (1991): "Preliminary Results From an Airdata Enhancement Algorithm with Application to High Angle-of-Attack Flight", AIAA-91-0672, 29th Aerospace Sciences Meeting, Reno, NV, January 7-10.

Murrow, H.N., and R.H. Rhyne (19xxx): "Flight Instrumentation for Turbulence Measurements in the Atmosphere", Personal correspondence, NASA Langley Research Center, Hampton, VA.

NSTS 08211 (1988): "Launch Systems Evaluation Advisory Team (LSEAT) Integrated Support Plan", Lyndon B. Johnson Space Center, Houston, TX, July 25.

O'Donnell, C.F., eds. (1964): Inertial Navigation - Analysis and Design, McGraw-Hill Book Company, Inc., New York, NY.

Parish, T.R., and D.H. Bromwich (1989): "Instrumented Aircraft Observations of the Katabatic Wind Regime Near Terra Nova Bay", Monthly Weather Review, Vol. 117, pp. 1570-1585.

Pitman, G.R., Jr., eds. (1962): Inertial Guidance, John Wiley & Sons, Inc., New York, NY.

Poellet, M. (1990): "University of North Dakota Cessna Citation II", Personal correspondence, August.

Potter, G.G. (1982): "A Sensitivity Analysis of the Kalman Filter as Applied to an Inertial Navigation System", Naval Postgraduate School Thesis, Monterey, CA, June.

Puckett, A.E., and S. Ramo (1959): Guided Missile Engineering, McGraw-Hill Book Company, Inc., New York, NY.

Renard, R.J., and M.S. Foster (1978): "The Airborne Research Data System (ARDS): Description and Evaluation of Meteorological Data Recorded During Selected 1977 Antarctic Flight", Rep. No. NPS 63-78-002, Naval Postgraduate School, Monterey, pp. 90.

Rhyne, R.H. (1980): "Accuracy of Aircraft Velocities Obtained From Inertial Navigation Systems for Application to Airborne Wind Measurements", NASA TM-81826, July.

Rider, C.K., M.R. Thomson, and F.E. Verinder (1971): "Measurement of Extreme Mechanical Turbulence During Low Level Flights by Mirage A3-76", Department of Supply, Australian Defense Scientific Service, Structures and Materials Report 333.

Ringnes, E.A., and W. Frost (1985): "Analysis of Aerodynamic Coefficients Using Gust Gradient Data: Spanwise Turbulence Effects on Airplane Response." NASA CR-3961.

Sakamoto, G.M. (1976): "Aerodynamic Characteristics of a Vane Flow Angularity Sensor System Capable of Measuring Flightpath Accelerations for the Mach Number Range from 0.40 to 2.54", NASA TN D-8242, May.

Scott, S.G., T.P. Bui, K.R. Chan, and S.W. Bowen (1988): "The Meteorological Measurement System on the NASA ER-2 Aircraft", submitted to the Journal of Geophysical Research.

Scott, S.G., T.P. Bui, R. Chan, and S.W. Bowen (1989): "The Meteorological Measurement System on the NASA ER-2 Aircraft." NASA Ames Research Center, Moffet Field, CA, June.

Shaw, W.A. (1966): "Developments in Theoretical and Applied Mechanics", Vol. 3, proceedings of the Third Southeastern Conference on Theoretical and Applied Mechanics, University of South Carolina, March 31-April 1.

Shibata, M. (1986): "Error Analysis Strapdown Inertial Navigation Using Quaternions", Journal of Guidance, Control, and Dynamics, Vol. 9, No. 3, pp. 379, May-June.

Schuler, M. (1923): "Die Storung von Pendelund Kreiselapparaten durch die Beschleunigung des Fahrzeuges, Physik Z., Vol. 24, July. A translation appears in Inertial Guidance (G.R. Pittman, Jr., ed.). John Wiley & Sons, Inc., New York, NY.

Stromberg, I.M., C.S. Mill, T.W. Choularton, and M.W. Gallagher (1989): "A Case Study of Stably Stratified Airflow Over the Pennines Using An Instrumented Glider", Boundary-Layer Meteorology, Vol. 46, pp. 153-168.

System Technical Description - Carousel IV Inertial Navigation System, A.C. Electronics, Division of General Motors Corp.

Telford, J.W., and P.B. Wagner (1974): "The Measurement of Horizontal Air Motion near Clouds from Aircraft", Journal of the Atmospheric Sciences, Vol. 31, No. 8, pp. 2066-2080.

Telford, J.W., P.B. Wagner, and A. Vaziri (1977): "The Measurement of Air Motion from Aircraft", Journal of Applied Meteorology, Vol. 16, pp. 156-166.

Waco, D.E., (1979): "Meteorological and Opertional Aspects of 46 Clear Air Turbulence Sampling Missions with an Instrumented B-57B Aircraft, Volume II (Appendix C) - Turbulence Missions", prepared for NASA Langley Research Center, NASA TM-80045.

Weber, O. (1975): "Statistical Studies on the Accuracy of Carousel IV Inertial Navigation Systems After Flights Over the North Atlantic", ERSO TT-136, West Germany.

Weinreb, A., and I.Y. Bar-Itzhack (1978): "The Psi-Angle Error Equation in Strapdown Inertial Navigation Systems", IEEE Transactions on Aerospace and Electronic Systems, Vol. AES-14, No. 3, pp. 539-544, May.

Winebarger, R.M. (1986): "Loads and Motions of an F-106B Flying Through Thunderstorms", NASA TM-87671, May.

Woodfield, A.A., and J.M. Vaughn (1983): "Airspeed and Wind Shear Measurements with an Airborne CO_2 Continuous Wave Laser", Royal Aircraft Establishment, TR-83061, July.

Yamamoto, S., et al. (1977): "Airborne Measurments of Turbulence heat Fluxes", J. Meteor. Soc., Japan, 55.

Yokoyama, O., et al. (1977): "On the Turbulent Quantities in the Atmospheric Mixing Layer", J. Meteor. Soc., Japan, 55.

Yokoyama, O., et al. (1977): "On the Turbulent Quantities in the Neutral Atmospheric Boundary Layer", J. Meteor. Soc., Japan, 55.

APPENDIX A

Wind Vector Calculations from an Airborne Platform

Windspeed and direction, based on measurements made from an airborne platform, are calculated from the vector addition

$$\vec{W} = \vec{V}_e - \vec{V}_a \qquad (A.1)$$

where $\vec{W}$ is the wind velocity with respect to an observer on earth, $\vec{V}_a$ is the air velocity according to an observer on the airborne platform, and $\vec{V}_e$ is the platform velocity in the frame of the earth. Measurements from the platform provide the information for airspeed and direction in a coordinate system that rolls, pitches, and yaws with the platform. An inertial measurement system on board the aircraft measures the angles, angular velocity, and linear velocity which describe the platform motion and orientation with respect to the earth. With the airflow vector known in the moving coordinate system and the orientation of the moving coordinate system with respect to the earth known, the wind vector in the earthbound coordinate system can be calculated.

A.1 Body-Fixed Frame

Airspeed in the coordinate system fixed to an aircraft (the true airspeed of the aircraft), is calculated from total pressure, ambient pressure, and total temperature measurements. Etkin (1973) calls this coordinate system the body-fixed coordinates, which is defined as having the x-axis pointing forward through the aircraft nose along the aircraft centerline, the y-axis pointing out the starboard wing, and the z-axis pointing out the aircraft underside. The origin of the coordinate system is located at the aircraft center of gravity.

The magnitude of the relative speed of the air to the aircraft, $|V_a|$, is determined

from the Mach number, Ma, and the sonic speed, c, by:

$$V_a = cMa \qquad (A.2)$$

The Mach number of the airplane is calculated from the total and ambient pressures according to the expression

$$Ma = \sqrt{\left[\left(\frac{p_0}{p}\right)^{\frac{k-1}{k}} - 1\right]\left[\frac{2}{k-1}\right]} \qquad (A.3)$$

where p_0 is the total pressure, p is the ambient pressure, k is the ratio of specific heats for air (1.4), and Ma represents the Mach number.

The total pressure and static pressure measurements, or pitot measurements, are taken, respectively, where the airflow is brought adiabatically and isentropically to rest and where the flow speed is undisturbed from the free stream flow. When the vehicle is traveling supersonically, a shock wave in front of the rocket or attached to the rocket will reduce the total pressure and increase the static pressure, compared to the total pressure and static pressure on the supersonic side of the shock wave. The subsonic Mach number calculated from Equation (A.3) is subsequently less than the free stream Mach number. The shock wave in front of the total and static pressure transducers, mounted on the rocket nose cone or at the end of a boom, is assumed to be a normal shock wave. For the airspeed calculation, the free stream Mach number (on the supersonic side of the shock wave) is calculated from the measured total pressure and measured static pressure from

$$Ma_2^2 = \left[\left(\frac{p_o}{p}\right)^{\frac{k-1}{k}} - 1\right]\left[\frac{2}{k-1}\right] \qquad (A.4)$$

and

$$Ma_1^2 = \frac{(k-1)Ma_2^2 + 2}{2kMa_2^2 - (k-1)} \qquad (A.5)$$

67

where Ma_2^2 = subsonic Mach number squared at the sensor, and Ma_1^2 = supersonic free stream Mach number squared.

The sonic speed is defined by

$$c = \sqrt{kRT} \qquad (A.6)$$

where R is the ideal gas constant for air, and T is the static temperature of the air.

Since only total temperature can be measured, the static temperature of the air is calculated from the relationship between the known Mach number, the total temperature, and the static temperature:

$$T = T_o \left[1 + \frac{k-1}{2} Ma^2 \right]^{-1} \qquad (A.7)$$

where T_o is the airstream total temperature.

With static temperature calculated, the sonic speed can be calculated from Equation (A.5) and airspeed is calculated from Equation (A.4). The airstream speed is then calculated from total pressure, static pressure, and total temperature from the expression

$$V_a = \left(\frac{p_o}{p} \right)^{-\frac{k-1}{2k}} \sqrt{kRT_o} \sqrt{ \left[\left(\frac{p_o}{p} \right)^{\frac{k-1}{k}} - 1 \right] \left[\frac{2}{k-1} \right] } \qquad (A.8)$$

The direction of the air relative to a probe is fixed by the angle-of-attack, α, and sideslip angle, β. In the body-fixed coordinate system the components of the relative airspeed vector are:

$$V_{BF} = |V_a| \begin{pmatrix} \cos\alpha \cos\beta \\ \cos\alpha \sin\beta \\ \sin\alpha \end{pmatrix} \qquad (A.9)$$

The Dryden F-104 and the Ames ER-2 use different methods for measuring α and β. The Dryden F-104 uses flow vanes such as shown in Figure A.1, and the Ames ER-2 uses differential pressure measurements on the radome (Figure A.2) which are correlated to particular flow angles.
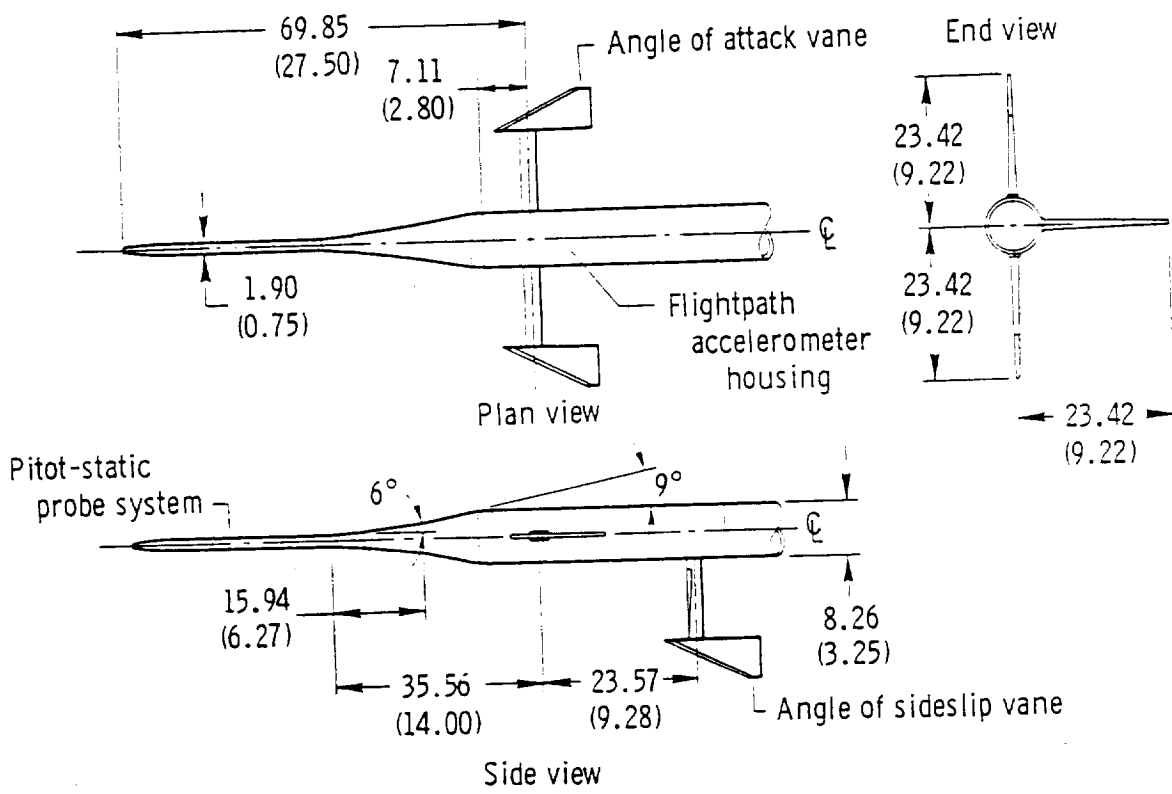
Figure A.1 Free vanes on an air data probe for flow angle measurements (Sakamoto , 1976).

69

Figure A.2 ER-2 radome with angle-of-attack and sideslip angle pressure ports (Scott, et al., 1989).

70

The standard NACA airdata probe, which is used by the Dryden F-104, is equipped with vanes which measure airflow direction by vane displacement. The actual flow angle is found by correcting the displacement angle according to wind tunnel calibrations for varying Mach number, angle-of-attack and sideslip. Figure A.3 shows typical flow angle errors and indicated flow angles (Sakamoto, 1976).

Similarly to the differential pressure measurement system on the ER-2, probes are designed to measure flow angles and flight Mach number for aircraft and wind tunnels from differential pressure measurements. Such a probe, with a hemispherical head, is illustrated in Figure 2.2. A flow angle in a given plane would be calculated from (see Scott, et al. (1989))

$$\alpha = \frac{\Delta p}{kq} \qquad (A.10)$$

where α is the flow angle, Δp is the differential pressure, k is the airflow angle sensitivity factor, and q is the dynamic pressure, $p_o - p$. The airflow angle sensitivity factor would be found from wind tunnel calibrations and is roughly constant within small Mach number domains. Bryer and Pankhurst (1971) recommended that for high subsonic, transonic, and low supersonic measurements, a hemispherical probe be used (Figure 2.2).

Before the air velocity is transformed into the earth-surface coordinates, with the x-axis pointed north, the y-axis pointed east, the z-axis pointed down, and the origin fixed to an observer on earth, the vehicle rotation rate must be accounted for in the body-fixed frame. The instruments that measure the pressures and angles necessary for the wind vector calculation rotate around the vehicle center of gravity. The linear velocity of the instruments due to the vehicle rotation is

$$\vec{V}_r = \vec{\omega} \times \vec{r} = \begin{pmatrix} p \\ q \\ r \end{pmatrix} \times \vec{r} \qquad (A.11)$$
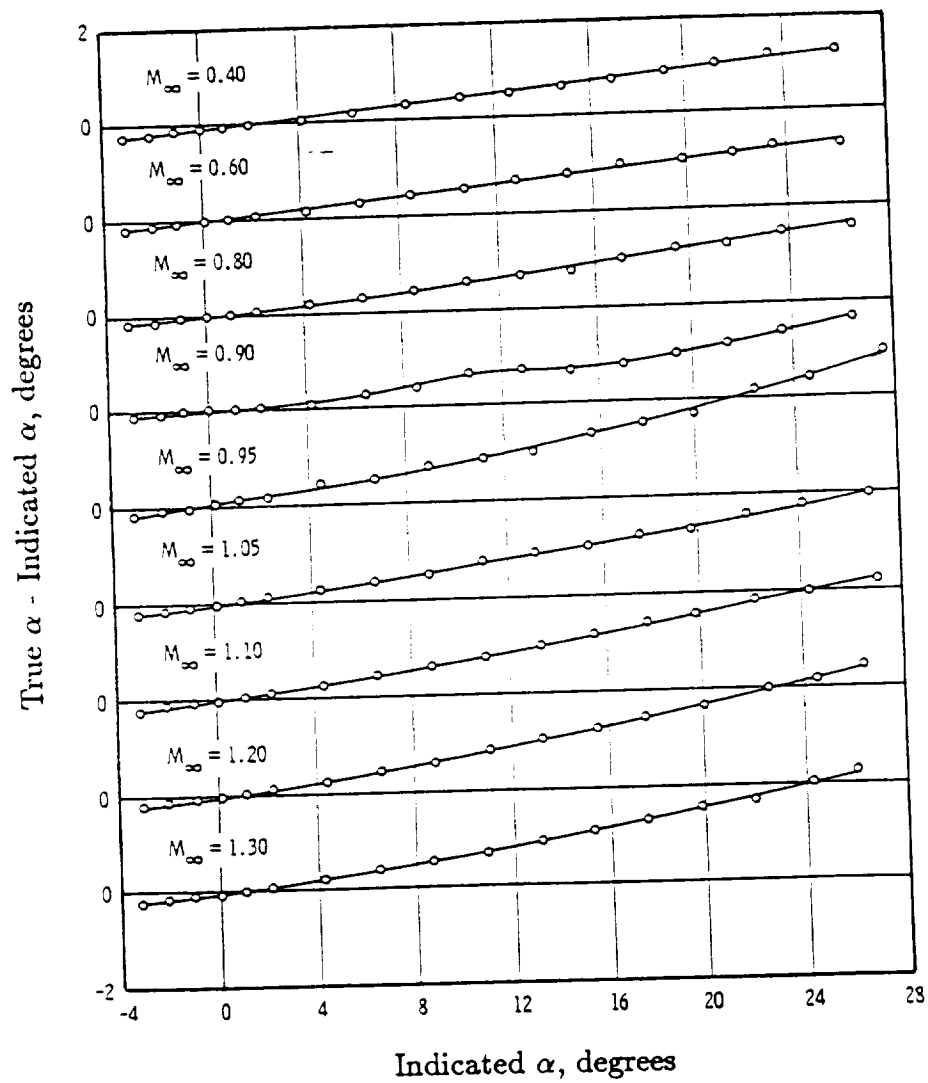
Figure A.3 Typical flow angle error from free vanes (Sakamoto,1976).

where p is the vehicle rate of roll, q is the vehicle rate of pitch, r is the vehicle rate of yaw, and $\vec{r}$ is the position vector of the instruments. The instrument velocity vector must be added to the relative airspeed velocity vector. The air velocity to be transformed from the body-fixed to an intermediate frame (the vehicle-centered vertical frame) is then

$$\vec{V} = |V_a| \begin{pmatrix} \cos\alpha\cos\beta \\ \cos\alpha\sin\beta \\ \sin\alpha \end{pmatrix} + \vec{\omega} \times \vec{r} \qquad (A.12)$$

A.2 Vehicle-Centered Vertical Frame

The vehicle-centered vertical frame, as defined by Etkin (1972), has its origin fixed at the aircraft center of gravity, with the x-axis pointed north, the y-axis pointed east, and the z-axis pointed in the direction of the local gravity vector. Etkin (1972) gives the transformation of vector components from a body-fixed to a vehicle-centered vertical coordinates as

$$V_{VC} = \begin{pmatrix} \cos\theta & \begin{matrix} \sin\phi\sin\theta\cos\Psi \\ -\cos\phi\sin\Psi \end{matrix} & \begin{matrix} \cos\phi\sin\theta\cos\Psi \\ +\sin\phi\sin\Psi \end{matrix} \\ \cos\theta\sin\Psi & \begin{matrix} \sin\phi\sin\theta\sin\Psi \\ +\cos\phi\cos\Psi \end{matrix} & \begin{matrix} \cos\phi\sin\theta\sin\Psi \\ -\sin\phi\cos\Psi \end{matrix} \\ -\sin\theta & \sin\phi\cos\theta & \cos\phi\cos\theta \end{pmatrix} V_{BF} \qquad (A.13)$$

where ϕ = aircraft roll angle, θ = pitch angle, and Ψ = yaw angle. The angles ϕ, θ, and Ψ, called the Euler angles.

These angles are typically provided by gyroscopic measurements from an inertial navigation system (INS).

A.3 Earth-Surface Frame

The vehicle-centered vertical frame and the earth-surface frame differ only in the relative velocity between their respective origins. Thus the transformation of a vector from the former to the latter involves only the addition of the velocity of the vehicle-centered vertical frame relative to earth-surface. This relative velocity is simply the ground speed of the vehicle:

73

$$\vec{W} = \vec{V}_e - \vec{V}_a \qquad\qquad (A.14)$$

The vehicle ground speed is determined by integration of acceleration measurements on the aircraft. Typically, an INS provides velocity information in the earth-surface frame. If acceleration measurements only are used they are transformed from the frame of the vehicle to the earth-surface frame by the same vector transformation used with the calculated air velocity.

APPENDIX B

Error Analysis for Instrumentation Requirements for Wind Velocity Calculation from Measurements Made from an Airborne Platform

The uncertainty in the calculation of a wind vector from measurements made on an airborne platform is determined herein with the Taylor series error propagation approximation

$$(\Delta F)^2 = \sum_{i=1}^{n} \left(\frac{\partial F}{\partial \xi_i}\right)^2 \left(\Delta \xi_i\right)^2 \qquad (B.1)$$

where F is the parameter of interest and the set of ξ_i are the independent variables governing F.

In the case of wind calculations from an airborne platform, the platform being an airplane or a rocket, Equation (B.1) becomes:

$$|\Delta \vec{W}|^2 = |\Delta \vec{V_e} - \Delta \vec{V_a}|^2 \qquad (B.2)$$

where $\vec{W}$ is the wind vector, $\vec{V_e}$ is the inertial velocity vector of the vehicle (or ground speed) in the earth- surface frame, and $\vec{V_a}$ is the relative airspeed vector. The inertial velocity, which is determined by an INS, radar, radio navigation, or other means, and is treated in this analysis as a given function of the instrumentation.

The earth-surface frame is defined as a Cartesian coordinate system with the x-axis pointed north, the y-axis pointed east, and the z-axis pointed down. The origin of the earth-surface frame is arbitrary since the wind vector is a velocity rather than a position. The earth-surface frame is not considered curvilinear here, since the earth can be approximated as flat for the spatial scale of interest.

The error in the vehicle ground speed vector, $\Delta \vec{V_e}$, which is dependent on the instrumentation used for that measurement, is an independent variable in the error analysis. The relative air velocity vector is also an independent variable in the error analysis and is a function of the inaccuracies of the relative airspeed

75

instrumentation. The error analysis is best carried out in terms of components in the particular reference frames of interest. Toward this goal the relative airspeed vector components typically measured in the body-fixed frame are transformed into the earth fixed frame. The matrix equation is:

$$V_{a_{EF}} = L_{VB} \ V_{a_{BF}} \qquad (B.3)$$

where $V_{a_{BF}}$ is the relative airspeed column matrix of components measured in the body-fixed frame, and L_{VB} is the transformation matrix which rotates a vector in the body-fixed frame to the earth fixed frame.

The body-fixed frame is defined, in terms of an aircraft, as having the x-axis projected from the aircraft nose along the fuselage centerline, the y-axis projected from the starboard wing, the z-axis projected from the aircraft underside. The origin of the coordinate system is at the aircraft center of gravity. Etkin (1973) derives the transformation matrix L_{VB} as:

$$L_{VB} = \begin{pmatrix} \cos\Psi & \begin{matrix} \sin\phi\sin\theta\cos\Psi \\ -\cos\phi\sin\Psi \end{matrix} & \begin{matrix} \cos\phi\sin\theta\cos\Psi \\ +\sin\phi\sin\Psi \end{matrix} \\ \cos\theta\sin\Psi & \begin{matrix} \sin\phi\sin\theta\sin\Psi \\ +\cos\phi\cos\Psi \end{matrix} & \begin{matrix} \cos\phi\sin\theta\sin\Psi \\ -\sin\phi\cos\Psi \end{matrix} \\ -\sin\theta & \sin\phi\cos\theta & \cos\phi\cos\theta \end{pmatrix} \qquad (B.4)$$

where ϕ is aircraft bank, θ is aircraft elevation, and Ψ is aircraft heading.

The components of $\vec{V}_a$, in the body fixed coordinates, are defined for convenience as

$$V_{a_{BF}} = (V_x, V_y, V_z) \qquad (B.5)$$

and the error as

$$\Delta V_{a_{BF}} = (\Delta V_x, \Delta V_y, \Delta V_z) \qquad (B.6)$$

The components of $\vec{V}_a$, in the earth fixed coordinates or vehicle centered coordinates, are defined as

$$V_{a_{VC}} = (V_x', V_y', V_z') \qquad (B.7)$$

76

and

$$\Delta V_{avc} = (\Delta V'_x, \Delta V'_y, \Delta V'_z) \qquad (B.8)$$

Three equations result from the expansion of Equation (B.3) with substitution into Equation (B.1) . Using index notation, these equations are

$$(\Delta V'_j)^2 = \left(\frac{\partial V'_j}{\partial V_i}\right)^2 (\Delta V_i)^2 + \left(\frac{\partial V'_j}{\partial X_i}\right)^2 (\Delta X_i)^2 \qquad (B.9)$$

where $X_1 = \phi$, $X_2 = \theta$, and $X_3 = \Psi$.

The derivatives on the R.H.S. of Equation (B.9) for $\Delta V'_x$ are

$$\frac{\partial V'_x}{\partial V_x} = \cos\theta \cos\Psi \qquad (B.10)$$

$$\frac{\partial V'_x}{\partial V_y} = \sin\phi \sin\theta \cos\Psi - \cos\theta \sin\Psi, \qquad (B.11)$$

$$\frac{\partial V'_x}{\partial V_z} = \cos\phi \sin\theta \cos\Psi + \sin\phi \sin\Psi, \qquad (B.12)$$

$$\frac{\partial V'_x}{\partial\phi} = V_y(\cos\phi \sin\theta \cos\Psi + \sin\phi \sin\Psi) \\ - V_z(\sin\phi \sin\theta \cos\Psi + \cos\phi \sin\Psi), \qquad (B.13)$$

$$\frac{\partial V'_x}{\partial\theta} = - V_x(\sin\theta \cos\Psi) + V_y \sin\phi \cos\theta \cos\Psi \\ + V_z \cos\phi \cos\theta \cos\Psi, \qquad (B.14)$$

and

$$\frac{\partial V'_x}{\partial\Psi} = - V_x \cos\theta \sin\Psi - V_y(\sin\phi \sin\theta \sin\Psi + \cos\phi \cos\Psi) \\ + V_z(- \cos\phi \sin\theta \sin\Psi + \sin\phi \cos\Psi) \qquad (B.15)$$

The derivatives on the R.H.S. of Equation (B.9) for $\Delta V'_y$ are

$$\frac{\partial V'_y}{\partial V_x} = \cos\theta \sin\Psi, \qquad (B.16)$$

$$\frac{\partial V'_y}{\partial V_y} = \sin\phi \sin\theta \sin\Psi + \cos\phi \cos\Psi, \qquad (B.17)$$

$$\frac{\partial V'_y}{\partial V_z} = \cos\phi \sin\theta \sin\Psi - \sin\phi \cos\Psi, \qquad (B.18)$$

77

$$\frac{\partial V_y'}{\partial \phi} = V_y(\cos \phi \sin \theta \sin \Psi - \sin \phi \cos \Psi)$$
$$+ V_z(-\sin \phi \sin \theta \sin \Psi - \cos \phi \cos \Psi), \qquad (B.19)$$

$$\frac{\partial V_y'}{\partial \theta} = - V_x \sin \theta \sin \Psi + V_y \sin \phi \cos \theta \sin \Psi$$
$$+ V_z \cos \phi \cos \theta \sin \Psi, \qquad (B.20)$$

and

$$\frac{\partial V_y'}{\partial \Psi} = V_x \cos \theta \cos \Psi + V_y(\sin \phi \sin \theta \cos \Psi - \cos \phi \sin \Psi)$$
$$+ V_z(\cos \phi \sin \theta \cos \Psi + \sin \phi \sin \Psi) \qquad (B.21)$$

The derivatives on the R.H.S. of Equation (B.9) for $\Delta V_z'$ are

$$\frac{\partial V_z'}{\partial V_x} = - \sin \theta, \qquad (B.22)$$

$$\frac{\partial V_z'}{\partial V_y} = \sin \phi \cos \theta, \qquad (B.23)$$

$$\frac{\partial V_z'}{\partial V_z} = \cos \phi \cos \theta, \qquad (B.24)$$

$$\frac{\partial V_z'}{\partial \phi} = V_y \cos \phi \cos \theta - V_z \sin \phi \cos \theta, \qquad (B.25)$$

$$\frac{\partial V_z'}{\partial \theta} = -V_x \cos \theta - V_y \sin \phi \sin \theta - V_y \cos \phi \sin \theta, \qquad (B.26)$$

and

$$\frac{\partial V_z'}{\partial \Psi} = 0 \qquad (B.27)$$

With the assumption that the uncertainties in the Euler angles are approximately equal, Equations (B.10) - (B.27) can be simplified by inspection after substituting the small angle assumption for the bank, ϕ, elevation, θ, and heading, ψ, angles to:

$$|\Delta V_{a_{VC}}|^2 = |\Delta V_{a_{BF}}|^2 + 2(\Delta \phi)^2$$

The error in the angle measurements are considered equal, i.e., $\Delta \phi = \Delta \psi = \Delta \theta$. The uncertainty in the angles ϕ, θ, and Ψ is dependent on the instruments, usually

gyroscopes, which are used to measure those angles and thus, $\Delta\phi$, $\Delta\theta$, and $\Delta\Psi$ are independent variables in the error analysis.

At this point, the rotation rate of the vehicle should be considered in the error analysis. As the vehicle rotates, a wind vector is induced at the windspeed instrumentation proportional to the rotation rate and the distance between the aircraft center of gravity (c.g.) and the windspeed instrumentation. However, the product of the rotation rate and length between the c.g. and instrumentation is normally small and the contribution to the measured windspeed is not significant. Thus, the error contributed by the measured rate of the vehicle rotation will be neglected here.

The three components of the relative airspeed vector in the body-fixed frame, V_x, V_y, and V_z, are derived from the magnitude of the airspeed $|V_a|$, the angle-of-attack, α, and sideslip angle, β:

$$\begin{pmatrix} V_x \\ V_y \\ V_z \end{pmatrix} = |V_a| \begin{pmatrix} \cos\alpha\cos\beta \\ \cos\alpha\sin\beta \\ \sin\alpha \end{pmatrix} \qquad (B.28)$$

The resultant errors in the calculations of the body-fixed wind vector components are:

$$(\Delta V_x)^2 = \cos^2\alpha\cos^2\beta(\Delta|V_a|)^2 + |V_a|^2 \sin^2\alpha\cos^2\beta(\Delta\alpha)^2$$
$$+ |V_a|^2\cos^2\alpha\sin^2\beta(\Delta\beta)^2, \qquad (B.29)$$

$$(\Delta V_y)^2 = \cos^2\alpha\sin^2\beta(\Delta|V_a|)^2 + |V_a|^2 \sin^2\alpha\cos^2\beta(\Delta\alpha)^2$$
$$+ |V_a|^2\cos^2\alpha\cos^2\beta(\Delta\beta)^2, \qquad (B.30)$$

and

$$(\Delta V_z)^2 = \sin^2\alpha(\Delta|V_a|)^2 + |V_a|^2\cos^2\alpha(\Delta\alpha)^2 \qquad (B.31)$$

Defining $|\Delta\vec{V_a}|^2 = (\Delta V_x)^2 + (\Delta V_y)^2 + (\Delta V_z)^2$, incorporating Equations (B.29), (B.30), and (B.31) and normalizing by the vehicle airspeed then with the small angle approximations, we can write:

$$\frac{|\Delta \vec{V_a}|^2}{|V_a|^2} = \left(\frac{\Delta |V_a|}{|V_a|}\right)^2 + 2(\Delta \alpha)^2 \qquad (B.32)$$

where it is assumed $\Delta \alpha = \Delta \beta$.

The errors in the measured angle-of-attack and sideslip angles are functions of the instruments used to make these measurements and are therefore independent variables.

The magnitude or absolute value of the airspeed of the vehicle, $|V_a|$, is calculated as the product of the local sonic velocity and the vehicle flight Mach number:

$$|V_a| = cMa \qquad (B.35)$$

For convenience which will become apparent, the square of the Mach number will be used:

$$|V_a| = c\sqrt{Ma^2} \qquad (B.36)$$

Then

$$(\Delta |V_a|)^2 = Ma^2(\Delta c)^2 + \frac{c^2}{4Ma^2}(\Delta Ma^2)^2 \qquad (B.37)$$

or

$$\left(\frac{\Delta |V_a|}{c}\right)^2 = Ma^2(\frac{\Delta c}{c})^2 + \frac{(\Delta Ma^2)^2}{4Ma^2} \qquad (B.38)$$

The sonic velocity, c, is calculated from the static temperature of the wind from

$$c = \sqrt{kRT} \qquad (B.39)$$

and

$$(\Delta c)^2 = \frac{kR}{4T}(\Delta T)^2 \qquad (B.40)$$

where $k = 1.4$ is the ratio of specific heats for air, and R is the perfect gas constant for air. Equation (B.40) can be rearranged from division by Equation (B.39) twice:

$$\left(\frac{\Delta c}{c}\right)^2 = \frac{1}{4}\left(\frac{\Delta T}{T}\right)^2 \qquad (B.41)$$

The static temperature is calculated from the Mach number and the total temperature, T_o, of the air surrounding the vehicle from the relationship

$$\frac{T_o}{T} = 1 + \frac{k-1}{2} Ma^2 \qquad (B.42)$$

Rearranging Equation (B.42) as

$$T = T_o \left(1 + \frac{k-1}{2} Ma^2\right)^{-1} \qquad (B.43)$$

and substituting into Equation (B.1)

$$(\Delta T)^2 = \frac{(\Delta T_o)^2}{(1 + \frac{k-1}{2} Ma^2)^2} + \frac{T_o^2 (\Delta Ma^2)^2}{(\frac{k-1}{2}(1 + \frac{k-1}{2} Ma^2)^2)^2} \qquad (B.44)$$

Equation (B.42) can be substituted back into Equation (B.44) for

$$(\Delta T)^2 = \frac{(\Delta T_o)^2}{(T_o/T)^2} + \frac{T_o^2 (\Delta Ma^2)^2}{(\frac{k-1}{2}(T_o/T)^2)^2} \qquad (B.45)$$

or

$$\left(\frac{\Delta T}{T}\right)^2 = \left(\frac{\Delta T_o}{T_o}\right)^2 + \frac{(\Delta Ma^2)^2}{\frac{(k-1)^2}{4}(1 + \frac{k-1}{2} Ma^2)^2} \qquad (B.46)$$

Since T_o is measured, T_o is an independent variable in the wind velocity calculations and the value of ΔT_o is dependent on the accuracy of the total temperature probe used for that measurement.

The Mach number is calculated as a function of the ratio of the dynamic and static pressure measured at the aircraft for subsonic flight by:

$$Ma^2 = \frac{2}{k-1} \left(\left(\frac{q}{p} - 1\right)^{\frac{k-1}{k}} - 1\right) \qquad (B.47)$$

If the system is flying supersonically, the free stream Mach number is calculated with the Rayleigh pitot-tube formula:

$$\frac{q}{p} + 1 = \left(\frac{k+1}{2} M_1^2\right)^{\frac{k}{k-1}} \bigg/ \left(\frac{2k}{k+1} M_1^2 - \frac{k-1}{k+1}\right)^{\frac{1}{k-1}} \qquad (B.48)$$

where Ma_1 = the supersonic free stream Mach number.

The uncertainty in the subsonic Mach number is calculated from Equation (B.47):

$$\left(\frac{\Delta Ma^2}{Ma^2}\right) = \left(\frac{\frac{2}{k}(1 + \frac{k-1}{2} Ma^2)^{\frac{k}{k-1}} - 1}{Ma^2}\right)^2 \left(\frac{\Delta \frac{q}{p}}{\frac{q}{p}}\right)^2 \qquad (B.50)$$

81

The uncertainty in the pressure ratio $\frac{q}{p}$ is evaluated from the two remaining independent variables in the wind velocity calculation

$$\left(\Delta\frac{q}{p}\right)^2 / \left(\frac{q}{p}\right)^2 = \left(\frac{\Delta p}{p}\right)^2 + \left(\frac{\Delta q}{q}\right)^2 \qquad (B.52)$$

Likewise, the uncertainty in the supersonic Mach number can be shown to be

$$\left(\frac{\Delta M^2}{M^2}\right)^2 = 2\left[\frac{M^2 - \frac{k-1}{2k}}{M^2 - \frac{1}{2}}\right]^2 \left[\frac{\frac{q}{p}}{\frac{q}{p} + 1}\right]^2 \left(\frac{\Delta p}{p}\right)^2$$

Finally, the uncertainty in wind velocity calculations from measurements made from a airborne platform is determined by the measured parameters $\vec{V}_e$, ϕ, θ, Ψ, T_o, p, p_o, α, and β, and their measurement uncertainties. This neglects any contribution to the wind velocity made by the rotation rate of the system, which is generally small.

Report Documentation Page

1. Report No.	2. Government Accession No.	3. Recipient's Catalog No.

4. Title and Subtitle

Guide to Measurement of Winds
With Instrumented Aircraft

5. Report Date

March 25, 1991

6. Performing Organization Code

FWG Associates, Inc.

7. Author(s)

Walter Frost
Terry S. Paige
Andrew E. Nelius

8. Performing Organization Report No.

10. Work Unit No.

9. Performing Organization Name and Address

FWG Associates, Inc.
217 Lakewood Drive
Tullahoma, TN 37388

11. Contract or Grant No.

NAS8-37893

13. Type of Report and Period Covered

12. Sponsoring Agency Name and Address   NASA
Washington, DC 20546-0001

NASA Marshall Space Flight Center
Marshall Space Flight Center, AL 35803

14. Sponsoring Agency Code

15. Supplementary Notes

16. Abstract

The salient features associated with measuring winds from aircraft are given. The report summarizes various techniques available and reviews some of the measurement programs for which instrumented aircraft have been developed and employed. A discussion is given of instrument types, potential sources of errors, and methods of correction and calibration.

The report is intended to provide a guide to researchers developing instrumented aircraft for measurement of atmospheric winds and related phenomena.

17. Key Words (Suggested by Author(s))		18. Distribution Statement
Aircraft	Turbulence	Unclassified - Unlimited
Instrumentation	Airborne Sensors	
Wind		

19. Security Classif. (of this report)	20. Security Classif. (of this page)	21. No. of pages	22. Price
Unclassified	Unclassified	88	

NASA FORM 1626 OCT 86